

See discussions, stats, and author profiles for this publication at: <https://www.researchgate.net/publication/349990468>

New Particle Formation and Growth to Climate-Relevant Aerosols at a Background Remote Site in the Western Himalaya

Article in *Journal of Geophysical Research Atmospheres* · April 2021

DOI: 10.1029/2020JD033267

CITATIONS

5

9 authors, including:



Vijay Kanawade
University of Hyderabad
95 PUBLICATIONS 2,133 CITATIONS

[SEE PROFILE](#)

READS

265



V. K. Soni
India Meteorological Department
83 PUBLICATIONS 1,237 CITATIONS

[SEE PROFILE](#)



Daniel McMahon Westervelt
Columbia University
29 PUBLICATIONS 923 CITATIONS

[SEE PROFILE](#)



A-P Hyvärinen
Finnish Meteorological Institute
140 PUBLICATIONS 4,254 CITATIONS

[SEE PROFILE](#)

Some of the authors of this publication are also working on these related projects:



Urban Meteorological Services [View project](#)



Absorbing Aerosols and Fate of the Indian Glaciers – AAFIG [View project](#)

New Particle Formation and Growth to Climate-relevant Aerosols at a background remote Site in the Western Himalaya

M. Sebastian¹, V. P. Kanawade^{1,*}, V. K. Soni², E. Asmi^{3,4}, D. M. Westervelt^{5,6}, V. Vakkari^{3,7}, A. -P. Hyvärinen³, J. R. Pierce⁸, and Rakesh K. Hooda³

¹Centre for Earth, Ocean and Atmospheric Sciences, University of Hyderabad, Hyderabad, India

²India Meteorological Department, Ministry of Earth Sciences, New Delhi, India

³Finnish Meteorological Institute, Erik Palmenin Aukio 1, Helsinki, Finland

⁴Servicio Meteorológico Nacional, Av. Dorrego, 4019, Buenos Aires, Argentina

⁵Columbia University, Lamont-Doherty Earth Observatory, NY, USA

⁶NASA Goddard Institute for Space Studies, New York, NY, USA

⁷Atmospheric Chemistry Research Group, Chemical Resource Beneficiation, North-West University, Potchefstroom, South Africa

⁸Department of Atmospheric Science, Colorado State University, Fort Collins, CO, USA

*Corresponding author: V. P. Kanawade (vijaykanawade03@yahoo.co.in)

Key Points:

- We present new measurement-based evidence of the contribution of new particle formation to climate-relevant aerosols in the Western Himalaya
- New particle formation occurred frequently in the pre-monsoon (March-May) season
- New particle formation rates were higher for cleaner events than polluted events

Keywords: new particle formation, particle growth, cloud condensation nuclei, the Himalaya

This article has been accepted for publication and undergone full peer review but has not been through the copyediting, typesetting, pagination and proofreading process, which may lead to differences between this version and the [Version of Record](#). Please cite this article as [doi: 10.1029/2020JD033267](https://doi.org/10.1029/2020JD033267).

This article is protected by copyright. All rights reserved.

Abstract

New particle formation (NPF) can influence the Earth's radiative budget when the newly formed particles grow to climate-relevant sizes. Here, we present analysis of 21-months of continuous aerosol size distribution measurements at a background remote site in the western Himalaya and provide observational evidence that newly formed particles grow to cloud condensation nuclei (CCN)-active sizes (i.e. >20 -100 nm in diameter). Out of total 55 NPF events, 38 (66%) events occurred in the pre-monsoon season (March-May). NPF events were classified into those with and without pollution influence as polluted and cleaner, respectively, using black carbon data. The analysis of air mass age, based on the ratio of number concentration of Aitken to accumulation mode aerosols, indicated that NPF occurred in the relatively cleaner air masses reaching to the site. The median formation rate of 10 nm particles and particle growth rates for cleaner events were three-fold and two-fold, respectively, higher than polluted events. We present the first estimates of the survival probability of newly formed particles to 50 nm and 100 nm size, which was not attempted in an Indian environment previously. The survival probability to 50 nm particles ranged from 44 to 98%, with a mean and standard deviation of $82 \pm 18\%$. On average, ~60% of the particles surviving to 50 nm survived to 100 nm, making the overall survival probability of 100 nm to $53 \pm 31\%$. This indicates that the probability of nucleated particles growing to CCN-active sizes under a large source of condensing vapor (transported from nearby lower-altitude regions) and low pre-existing particle concentrations (background mountain site) is high compared to the previous studies. These findings highlight the importance of the efficiency of nucleation events for producing CCN, which is a critical basis of aerosol indirect effects.

1 Introduction

Solid or liquid particles suspended in air are defined as atmospheric aerosols. Much has been learned about the effects of atmospheric aerosols on weather and climate. Aerosols affect weather, climate, human health, and air quality, thus it is of significant societal and economical importance [*Chowdhury et al., 2018; IPCC, 2013; Landrigan et al., 2018*]. Aerosols also counteract some fraction of greenhouse gas-driven global warming [*Paasonen et al., 2013*], by directly scattering and absorbing solar radiation and altering cloud properties [*Rosenfeld et al.,*

2014; *Sarangi et al.*, 2018]. Amongst current uncertainties in the radiative forcing, aerosol-induced changes in cloud properties is the largest source of uncertainty in future climate projections at the regional and global scales [IPCC, 2013].

Aerosol nucleation is the process of formation of new particles from vapors (hereafter referred to as new particle formation – NPF) and it is the largest source of aerosol numbers in the atmosphere [Kulmala *et al.*, 2013; Zhang *et al.*, 2012]. However, these newly formed aerosols of 1-2 nm in diameter need to grow further to climate-relevant cloud condensation nuclei (CCN) sizes (i.e. 50-100 nm in diameter) until they are able to influence clouds and thereby climate [Kerminen *et al.*, 2012; Wang and Penner, 2009], even though smaller aerosols affect human health, air quality, and atmospheric chemistry [Landrigan *et al.*, 2018; von Schneidemesser *et al.*, 2015]. NPF has been observed to take place throughout most of the terrestrial troposphere, including high altitude sites [Kerminen *et al.*, 2018; Sellegrí *et al.*, 2019]. Numerical experiments over the Midwestern USA, where NPF occurred frequently on regional scale, showed that NPF inhibits growth of pre-existing aerosols to CCN sizes by reducing ambient sulfuric acid concentrations over the region, and thereby the ambient CCN concentrations and cloud albedo, leading to an overall warming effect relative to when NPF was excluded [Sullivan *et al.*, 2018]. Westervelt *et al.* [2014] relates CCN formation to various nucleation schemes using simulation in GEOS-Chem-TOMAS global aerosol model and highlighted that nucleation contributed to about half of the CCN concentrations. A recent study also indicated that NPF produces about 54% of CCN in the present day with an estimated uncertainty range of 45-85% [Gordon *et al.*, 2017]. Thus, the contribution of NPF to the global CCN budget spans a relatively large range of uncertainty [Kerminen *et al.*, 2012; Westervelt *et al.*, 2014], which, together with our limited understanding of association between NPF and CCN, results in large uncertainties in the indirect radiative forcing by aerosols [IPCC, 2013]. Thus, the evident ubiquity and heterogeneity in linkages between NPF and CCN requires long-term continuous ambient observations, aided with state-of-the-art aerosol instrumentation techniques and regional to planetary scale model simulations to bring out new insights into field measurements.

The majority of comprehensive long-term ambient observations of NPF have been made in urban, rural, and remote areas in North America and Europe in locations that are more easily accessible [Hallas *et al.*, 2016; Kanawade *et al.*, 2012; Manninen *et al.*, 2010; Nieminen *et al.*, 2018]. NPF has also been studied at some high altitude sites, such as the measurements by

Venzac et al. [2008] at Himalayan Nepal Climate Observatory, Pyramid [NCO-P, 5079 m above mean sea level (amsl)] in the Khumbu Valley, *Kivekäis et al.* [2009] at Mount Waliguan (3816 m amsl), a remote mountain-top station in inland China, *Foucart et al.* [2018] at the Maïdo observatory (2150 m amsl), Réunion, a Southern Hemisphere site surrounded by Indian Ocean, *Venzac et al.* [2009] at the Puy de Dôme site (1465 m amsl) in France, *Boulon et al.* [2010] and *Tröstl et al.* [2016] at Jungfraujoch (3580 m amsl) in the Swiss Alps and *Hallar et al.* [2011] at Storm Peak Laboratory (3201 m amsl) in USA. Recently, *Sellegrí et al.* [2019] presented aerosol observations from six high altitude stations (Puy de Dôme in France, Mount Chacaltaya in Bolivian Andes, Nepal Climate Observatory Pyramid, Maïdo observatory on La Reunion Island in the Indian Ocean, Jungfraujoch in the Swiss Alps, and the Monte Cimone site on the Northern Apennines) for which a year-long measurements were available to derive statistically relevant NPF features (frequency, formation rates, growth rates and CCN contribution to total aerosols) and seasonal variability. Previous long-term studies from the Indian Himalaya have also characterized aerosol properties and NPF events such as the measurements by *Hooda et al.* [2018], *Neitola et al.* [2011] and [*Komppula et al.*, 2009] at Mukteshwar, a high altitude site (2180 m amsl) in North-western Indian Himalaya and *Moorthy et al.* [2011] at a high altitude site, Hanle (4520 m amsl), in the Trans-Himalaya. NPF frequency at Mukteshwar and Hanle sites in Himalaya showed a clear seasonal cycle that was connected to the evolution of atmospheric boundary layer and solar insolation, respectively. During the pre-monsoon season (March-May), the increasing boundary layer height lifted aerosols and their precursors from nearby lower-altitude regions up to the station, and the precursors combined with high solar insolation at the mountain top increased the NPF probability significantly [*Moorthy et al.*, 2011; *Neitola et al.*, 2011]. In addition, the ground-based NPF observations in India are limited to only a few locations, including Mahabaleshwar in Western Ghats [*Leena et al.*, 2017], New Delhi [*Mönkkönen et al.*, 2005], Kanpur and Pune [*Kamra et al.*, 2015; *Kanawade et al.*, 2020; *Kanawade et al.*, 2014a], Gadanki [*Kanawade et al.*, 2014b], and Trivandrum [*Babu et al.*, 2016]. However, none of the above previous studies in India, to our knowledge, has explored the linkage between atmospheric NPF and CCN formation.

In this study, we use 21-months (December 2016 – September 2018) of continuous aerosol size distribution measurements to establish statistics on NPF rates, growth rates, seasonal variability, survival probability, and CCN formation rates of newly formed aerosols to climate-

relevant aerosols at Ranichauri measurement site. In order to explain the seasonal variability in NPF features, different months are grouped in four seasons: winter (December–February), pre-monsoon (March–May), monsoon (June–September,) and post-monsoon (October and November).

2 Materials and Methods

2.1 Location

The village named Ranichauri is located in Tehri–Garhwal district of Uttarakhand state in the southern slope of the Western Himalaya. Figure 1a shows the location of Ranichauri and surrounding locations, including three high altitude sites in the Himalaya (Hanle, Mukteshwar, and NCO-Pyramid, Nepal) from where observations of aerosol size distributions were reported in the past. The observation site (30.2°N , 78.25°E ; ~ 1930 m amsl) is situated on an isolated hill-top, within the campus of College of Forestry in Ranichauri (Fig. 1b). The observation site is a Climate Monitoring station (hereafter referred to as Ranichauri) managed by India Meteorological Department (IMD) under the Global Atmospheric Watch (GAW) program of the World Meteorological Organization (WMO). The station is away from major sources of anthropogenic pollution and can be considered as a background observatory. But the black carbon (BC) concentrations measured at Ranichauri are considerably high for a background location (annual mean and standard deviation of $1.4 \pm 1.1 \mu\text{g m}^{-3}$). This is higher compared to a nearby high altitude remote site, Mukteshwar ($0.9 \pm 0.6 \mu\text{g m}^{-3}$) [Kumar *et al.*, 2020], particularly in the pre-monsoon season with the proximity of forest fires. The 10th, 25th, 50th, 75th, and 90th percentiles of BC at Ranichauri are 0.3, 0.6, 1.3, 2.1 and $3.2 \mu\text{g m}^{-3}$, respectively. The city of Rishikesh is located about 70 km to the south, Srinagar city about 100 km to the south-east and Dehradun city about 100 km to the west of Ranichauri. The topography of the region covers uneven distribution of forests, agriculture land, orchards, and small human settlements. Based on long-term observations (1985–2013), the daily maximum temperature varies from 9.4 to 27.2°C , with mean annual total rainfall of about 1274 mm at this site [Upadhyay *et al.*, 2015].

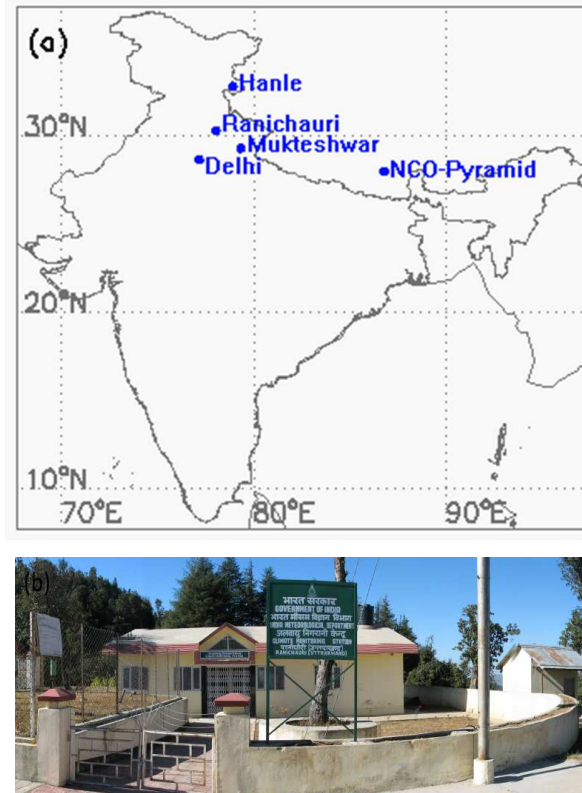


Figure 1. (a) Location of Ranichauri and surroundings locations, including high altitude sites in the Himalaya (b) Photograph of Ranichauri Climate Observing Station.

Air mass history was identified using HYSPLIT back trajectory calculations and ratio of number concentration of Aitken mode to accumulation mode aerosols. BC data was used to identify if the air mass reaching the site was polluted. Figure 2 shows the two-day backward trajectories of air masses arriving at 500 m above the ground at Ranichauri for winter, pre-monsoon, monsoon and post-monsoon seasons. Ranichauri generally experiences a mixture of relatively cleaner free tropospheric air and polluted air from highly polluted Indo-Gangetic Plain. During winter and post-monsoon seasons, the free tropospheric flow from north-western region predominantly reaches the site. Air masses from the polluted Indo-Gangetic Plain in the south-east were dominant during the pre-monsoon season whereas air masses from the south-east and west were prevalent during the monsoon season.

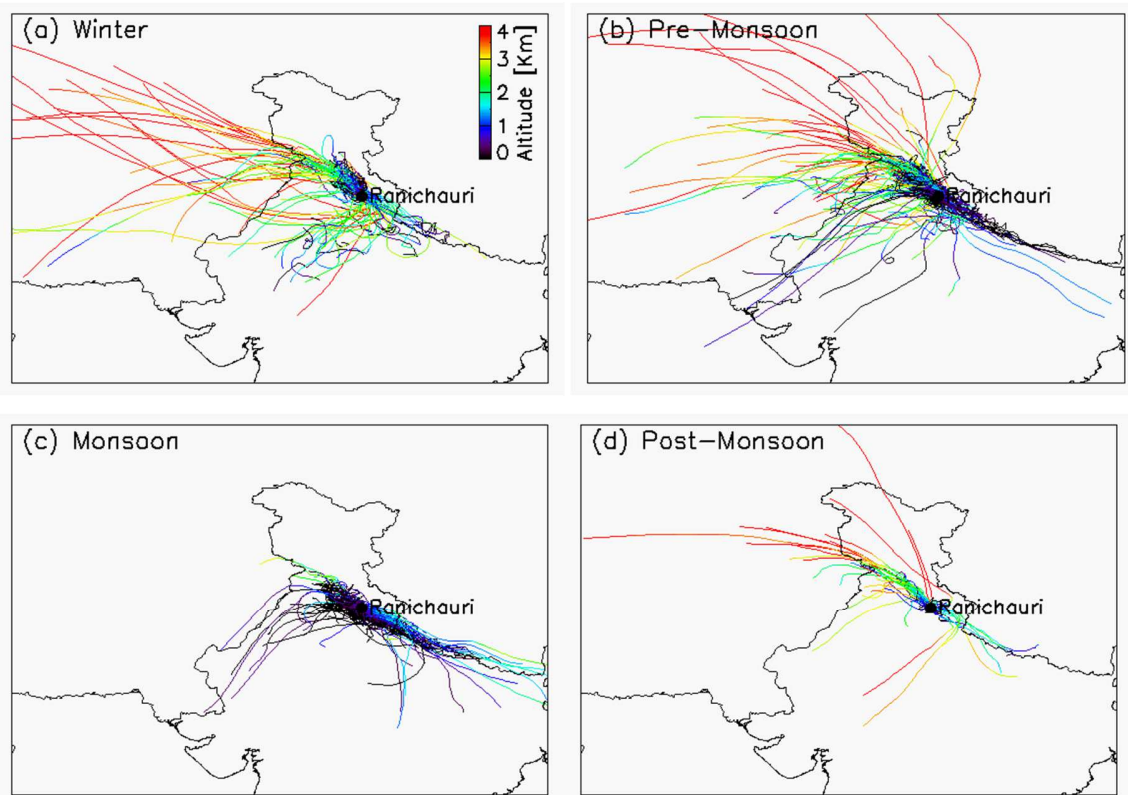


Figure 2. Two-day backward air mass trajectories starting at 500 m above the ground level for (a) winter (DJF), (b) pre-monsoon (MAM), (c) monsoon (JJAS) and (d) post-monsoon (ON) seasons. The color indicates the altitude along the air mass backward trajectory.

The Atmospheric Boundary Layer (ABL) influence was analysed using the methodology explained in *Hooda et al.* [2018]. It used specific humidity (q) as a passive tracer for ABL dynamics [Kowol-Santen *et al.*, 2001; Serafin *et al.*, 2018; Weigel *et al.*, 2007]. The lifting of air in the ABL was first assessed by examining the variability ' ∂q ' in specific humidity at two sites (Delhi and Ranichauri). Further, to investigate the ABL air lifting from the plains below, the hourly specific humidity difference between the two sites and corresponding undisturbed difference of q between Ranichauri and the plains (Delhi) 'denoted as ΔRPq ' was estimated. It was assumed, based upon ' ∂q ' diurnal-monthly values that there was no mixing of air happening at 5:00 am between the two sites (mountainous and plains). From these parameters, the fraction of air (Φq) arriving Ranichauri from the plains can be calculated as;

$$\Phi q = 1 - \frac{q_{DEL} - q_{RANI}}{\Delta RPq}$$

(1)

The influence of the Indo-Gangetic Plains boundary layer was evaluated with different threshold values of Φq (0.25, 0.5, and 0.75) and compared to the maximum mixing depth of Delhi (ERA-5 based) in terms of the fraction of the days (Fig. S1). More details are provided in supporting information.

2.2 Instrumentation and datasets

A custom-built differential mobility particle sizer (DMPS) was used to obtain the ambient aerosol size distribution in the size range of 10 nm to 800 nm (30 size bins). The DMPS consisted of a Vienna-type differential mobility analyzer (DMA) that classifies the charged particles according to their electrical mobility, and a TSI 3772 condensation particle counter (CPC) that counts particles of the selected mobility. Thus, the aerosol size information throughout the text is in electrical mobility diameter. A full aerosol number-size distribution with 30 bins was obtained every 10 minutes. The DMPS inlet flow rate was 1 liter per minute (LPM), and the sheath air flow rate was 5 LPM. The sample air was drawn inside through a stainless steel inlet tube of about 2 meter in length and dried to less than 40% relative humidity with a Nafion dryer. Diffusion losses in the inlet and inside the DMPS were considered in the data inversion. The inversion method was identical to that presented by *Wiedensohler et al.* [2012], for the Finnish Meteorological Institute (FMI) DMPS.

Black carbon measurements were made using Aethalometer (model AE-33)[*Magee Scientific*, 2016], which is deployed under IMD national network for measurements of BC at important geographical locations in India [*Kumar et al.*, 2020]. Aethalometer measures light attenuation at 7 wavelengths. The BC concentrations here are derived at a wavelength of 880 nm using mass absorption cross-section (MAC) value of $7.77 \text{ m}^2 \text{ g}^{-1}$ [*Petzold et al.*, 2013]. This wavelength was chosen to calculate BC concentration as absorption due to other aerosols is negligible at this wavelength [*Drinovec et al.*, 2015]. Aethalometer uses a Teflon-coated glass fiber tape and the aerosols are collected on a two parallel spot measurement of optical absorption, which provides near real-time compensation for the spot loading effect. Aethalometer inlet was equipped with an impactor for removing the aerosols with aerodynamic

Accepted Article

diameters larger than 2.5 μm . More details of BC measurement and calculation can be found in *Drinovec et al.* [2015].

Air mass origin and path to the measurement site were estimated using NOAA ARL PC-version Hybrid Single-Particle Lagrangian Integrated Trajectory (HYSPLIT) model [*Draxler and Rolph*, 2010] by calculating hourly two-day air mass backward trajectories starting at 500 m above the ground level using gridded wind fields from the Global Data Assimilation System (GDAS), which has a spatial resolution of $1^\circ \times 1^\circ$ longitude by latitude and a time resolution of 1 hour [*Kanamitsu*, 1989].

2.3 Estimation of relevant new particle formation features

We classified NPF events into different types upon visual inspection of the contour plot of the aerosol size distribution [*Dal Maso et al.*, 2005]. Particle mode diameter and BC concentrations were used to classify events into sub-types. To obtain the particle mode diameter (i.e. local maximum of the aerosol size distribution), multimodal log-normal distribution upto three modes was fitted to the measured aerosol size distribution. Type-I NPF events were identified by the presence of distinctly new mode of particles with diameters smaller than 25 nm and with a steady growth in diameter of this new mode for at least 6 hours such that aerosol size distributions displays a “banana” shaped aerosol growth. Type-I NPF events were further classified into two sub-types: Ia and Ib, based on BC concentrations. Type-Ia NPF event showed no or insignificant simultaneous increase in BC concentrations with new mode of particle diameter, implying a cleaner event (e.g. Fig.3a) whereas Type-Ib NPF event showed significant simultaneous increase in BC with the new mode of particle diameter, implying polluted event (e.g. Fig.3b). For these events, the particle growth rate (GR) was calculated by fitting a first-order polynomial line through growing particle mode diameter between 10 nm and 25 nm as a function of time and calculating its slope, following *Dal Maso et al.* [2005] methodology, modified and updated by *Westervelt et al.* [2013]. The formation rate of 10 nm particles (J_{10}) was found using the simplified approximation of the General Dynamic Equation (GDE), describing evolution of the aerosol size distribution. The formation rate of 10 nm particles was calculated from aerosol size distributions obtained from the DMPS (10-800 nm) using equation 2

$$J_{10} = \frac{dN_{10-25}}{dt} + F_{CoagS} + F_{growth} \quad (2)$$

where the first term in equation (2) is the rate of the change of nucleation mode particle number concentrations, the second term is the coagulation loss, and the third term is the flux out of the size range 10-25 nm i.e. condensational growth.

Type-II NPF events were similar to Type-I NPF events except that the initial mode diameter was larger than 25 nm. Thus, GR and J_{10} can not be calculated for Type-II NPF events. Such events are observed when the air mass with NPF reaches the measurement site after the particles have already grown larger than 25 nm, referred to as Aitken-mode growth events. Type-II NPF events were further classified into two sub-types: IIa (cleaner) and IIb (polluted), similar to Type-I NPF events. This indicates that Type-II events can occur in both cleaner and polluted air masses. Type-IIa NPF events showed no or insignificant simultaneous increase in BC concentrations, implying a cleaner event (e.g. Fig. 3c). Type-IIb NPF events showed simultaneous increase in BC concentrations, implying a polluted event (e.g. Fig. 3d). The days with no evidence of distinct change in particle mode diameter were identified as Type-III non-event (e.g. Fig. 3e). Those days, which were difficult to be classified as any one of the above categories, were identified as Type-IV unidentified event days (e.g. Fig. 3f). The criteria used for classifying these events are summarized in Table 1.

We also calculated size-segregated aerosol number concentrations by integrating the number concentration of aerosols from 10-25 nm (nucleation mode, N_{NUC}), 25-100 nm (Aitken mode, N_{AIT}), 100-800 nm (accumulation mode, N_{ACCU}) and 10-800 nm (total aerosols, N_{TOT}). Similarly, total aerosol surface area (SA_{TOT}), total volume (Vol_{TOT}), total mass concentration (M_{TOT}), total condensation sink (CS_{TOT}) and total coagulation sink ($CoagS_{TOT}$) in the size range of 10-800 nm were calculated following *Dal Maso et al.* [2005], to examine seasonal variability and diurnal patterns of NPF features. It is worth noting that there were no measurements of aerosols less than 10 nm diameter size during the study period. Therefore, it was not possible to precisely estimate the fraction of N_{NUC} originated from NPF processes, which usually starts at 1-2 nm diameter size [*Kulmala et al.*, 2007].

Table 1. Summary of new particle formation event classification.

Event type	subtype	features
Type-I NPF	Ia (cleaner)	A new mode of particles smaller than 25 nm size is visible with a steady growth in the particle size for at least 6 hours. GR and J_{10} can be calculated. No or insignificant simultaneous increase in BC concentrations with the particle mode diameter.
	Ib (polluted)	Same as Type-Ia, but with significant simultaneous increase in BC concentrations.
Type-II NPF	IIa (cleaner)	A new mode of particles smaller than 25 nm is absent referred to as Aitken-mode growth event. GR and J_{10} can not be calculated. No or insignificant simultaneous increase in BC concentrations with the particle mode diameter.
	IIb (polluted)	Same as Type-IIa, but with significant simultaneous increase in BC concentrations.
Type-III non-event		No distinct change in particle mode diameter during the course of the day
Type-IV unidentified		Difficult to identify whether it is one of the above event types.

2.4 Particle survival probability, CCN-active particle formation rates and CCN derived from SMPS

While particles as small as 20 nm may activate in summertime arctic clouds [Korhonen *et al.*, 2008; Leaitch *et al.*, 2016], in typical ambient in-cloud supersaturations, 50 nm and 100 nm can be considered as a good proxy for CCN concentration [Kerminen *et al.*, 2012] at approximately 1.0% and 0.2% supersaturation for stratiform clouds, respectively. Here, we have calculated the particle survival probabilities to 50 nm (SP50) and 100 nm (SP100) size following the methodology explained by Pierce and Adams [2007] and first applied to ambient observations in Westervelt *et al.* [2013]. Briefly, SP is the ratio of particle fluxes at the initial size and the CCN-active sizes (typically to 50 nm and 100 nm particles). The survival probability from initial size m to n (in this case, 10 to 50 nm and 10 to 100 nm) is calculated by the following equation:

$$SP_{m,n} = \prod_{k=m}^{n-1} \exp \left(-\frac{\tau_{k,k+1}^{cond}}{\tau_k^{coag}} \right) \quad (3)$$

where τ^{cond} is the condensational growth time scale required for a particle to grow to a size of interest. τ^{coag} is the inverse of the coagulation sink for a given size range. The formation rates of CCN-active particles (i.e. 50 nm and 100 nm) are calculated as, $J_{50} = J_{10} \times SP50$ and $J_{100} = J_{10} \times SP100$. J_{50} and J_{100} are the formation rate of particles of size 50 nm and 100 nm, respectively. While this methodology does not consider aerosol composition and mixing state, the particles larger than 50 nm will serve as CCN under typical supersaturations. Since, the aerosol size plays the major role in the aerosols ability to act as CCN rather than its composition [Dusek *et al.*, 2006]. The survival probabilities and formation rates of 50 nm and 100 nm particles were calculated for Type-I NPF event alone as it was not possible to derive J_{10} for Type-II NPF events.

We have also estimated the contribution of freshly formed particles to the CCN concentrations followed by Kerminen *et al.* (2012) methodology, which calculates $N_{CCNprior}$ and N_{CCNmax} . We used similar CCN thresholds i.e. 50 nm and 100 nm to calculate $N_{CCNprior}$ and N_{CCNmax} . $N_{CCNprior}$ is calculated as a one-hour average concentration immediately prior to the appearance of the newly formed nucleation mode particles, whereas N_{CCNmax} is calculated as a maximum one hour average concentration during an NPF event. The contribution of the nucleation to CCN concentrations during the observed Type-I NPF event days was then examined in both relative and absolute concentrations terms.

3. Results and Discussion

3.1 Typical NPF events and their frequency

Previous study at Nepal Climate Observatory at Pyramid (NCO-P) in the Khumbu Valley, a high altitude site in the Eastern Himalaya, using 16-months of aerosol size distributions showed that NPF events occurred very frequently when the more polluted air rising from valleys reach the site [Venzac *et al.*, 2008]. Whereas, the long-term (2005 - 2010) measurements of aerosol size distributions from Mukteshwar, Uttarakhand, a high altitude site in Western Himalaya, showed that the NPF events occurred rather sporadically, except during the pre-monsoon season [Neitola *et al.*, 2011]. NPF events during the pre-monsoon season were connected to the evolution of the boundary layer up to the site elevation.

Figure 3 shows typical NPF events observed at Ranichauri site. Type-Ia and Type-Ib are identical type of events except that BC concentrations did not vary during the course of Type Ia NPF event while BC concentrations increased sharply with particle mode diameter in case of Type-Ib NPF event. Many studies have suggested that NPF occur preferably at low aerosol loading, because high pre-existing aerosol concentrations tend to scavenge both nucleation precursors (e.g. sulfuric acid, ammonia, amines, and volatile organic compounds) and small molecular clusters [Kulmala *et al.*, 2004; Zhang *et al.*, 2012]. However, observations in polluted environments and plumes have also revealed significant rates of NPF despite the high ambient aerosol concentrations [Nie *et al.*, 2014; Nieminen *et al.*, 2018; Westervelt *et al.*, 2013; Yao *et al.*, 2018; Yu *et al.*, 2017; Zhang *et al.*, 2015]. Previous studies put forward the hypothesis that either reduced scavenging of nanometer-sized clusters to pre-existing aerosols or rapid cluster growth likely accounts for the nucleation and growth of nano particles in a polluted atmosphere [Dai *et al.*, 2017; Kulmala *et al.*, 2017]. These previous studies substantiate the Type-Ib events, which have NPF within a polluted air mass. The total condensation sink for Type-I NPF events were in the range $(1.2 - 52.8) \times 10^{-3} \text{ s}^{-1}$, with a mean and standard deviation of $(8.6 \pm 5.8) \times 10^{-3} \text{ s}^{-1}$. This value is higher by a factor of about three as compared to a high altitude site, Puy de Dôme in France ($2.77 \times 10^{-3} \text{ s}^{-1}$) and more than an order of magnitude higher than another high altitude site, Jungfraujoch in the Swiss Alps ($0.15 \times 10^{-3} \text{ s}^{-1}$) [Sellegrí *et al.*, 2019]. At the NCO-P site in the Khumbu Valley, Venzac *et al.* [2008] found that high pre-existing aerosol concentrations prevented NPF occurrence, with NPF frequencies less than 10% for condensation sink higher than $2.1 \times 10^{-3} \text{ s}^{-1}$, with a NPF frequency of about 50% for condensation sink lower than this value. This indicates that the typical condensation sink at Ranichauri site was sufficiently high that the natural source strength of vapors cannot overcome it and thereby inhibited cleaner NPF events. Type-II events (referred to as Aitken-mode growth events) were also sub-classified into IIa and IIb categories, similar to Type-I events. For the typical Type-Ia event shown in Figure 3, the calculated growth rate in the size range 10 - 25 nm diameter (8.45 nm h^{-1}) was almost two-fold than that of the Type-Ib event (4.69 nm h^{-1}). Overall, the growth rates for Type-Ia cleaner event days were higher than Type-Ib event days. In contrast, Neitola *et al.* [2011] reported higher growth rates at Mukteshwar site for boundary layer polluted events as compared to cleaner free tropospheric events.

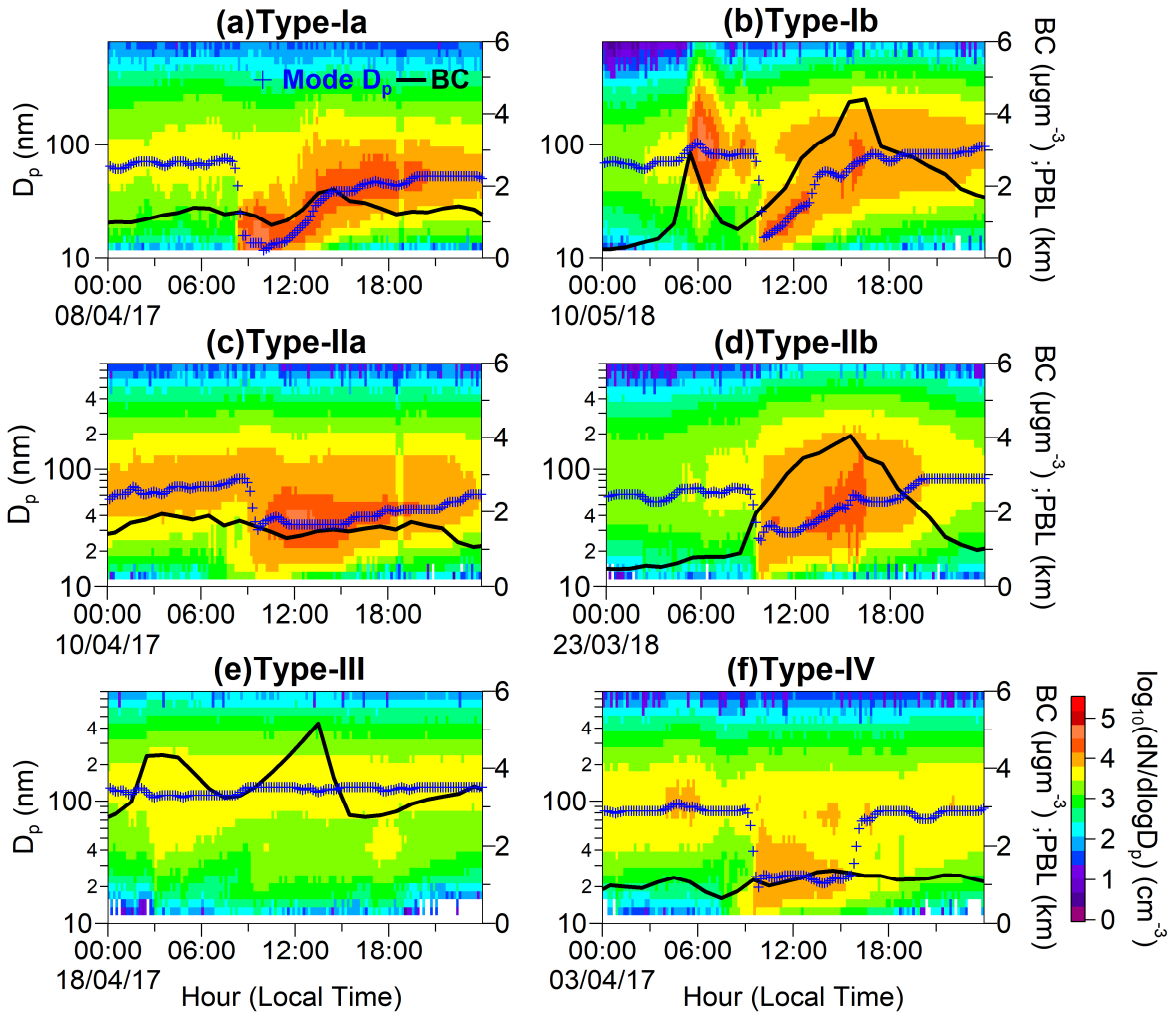


Figure 3. Temporal evolution of aerosol size distributions (filled contour), particle mode diameter (blue plus symbol), and BC mass concentrations (thick black line) for a typical Type-I NPF (a, b), Type-II NPF (c, d), Type-III non-event (e) and Type-IV unidentified (f) days at Ranichauri.

Figure 4 shows the percentage of days for different types of events observed at Ranichauri during the period of the study. Out of a total of 643 days of observations, there were 24 (3.6%) Type-I and 31 (4.8%) Type-II event days. A total of 493 (76.4%) days did not show any evidence of NPF and 33 (5.1%) days were categorised as unidentified days. There were no measurements on 62 (9.7%) days. The monthly percentage of occurrence of NPF days was comparable to an earlier study at a high altitude site, Mukteshwar, in the Western Himalaya [Neitola *et al.*, 2011], which is about 300 km to the Southeast of Ranichauri (Figure 1). Type-I

NPF events occurred frequently in the pre-monsoon season (23 out of a total 24 event days). The days with no evidence for NPF were more common in the monsoon season owing to wet/cloud scavenging of condensable vapours as well as small clusters, and low solar insolation on persistently cloudy conditions during the monsoon season. A study at a rural site, Gadanki, in India also observed infrequent occurrence of NPF connected to lower aerosol precursor concentrations and weak gas-phase oxidation due to diminished solar radiation on persistently cloudy days during monsoon season [Kanawade *et al.*, 2014b].

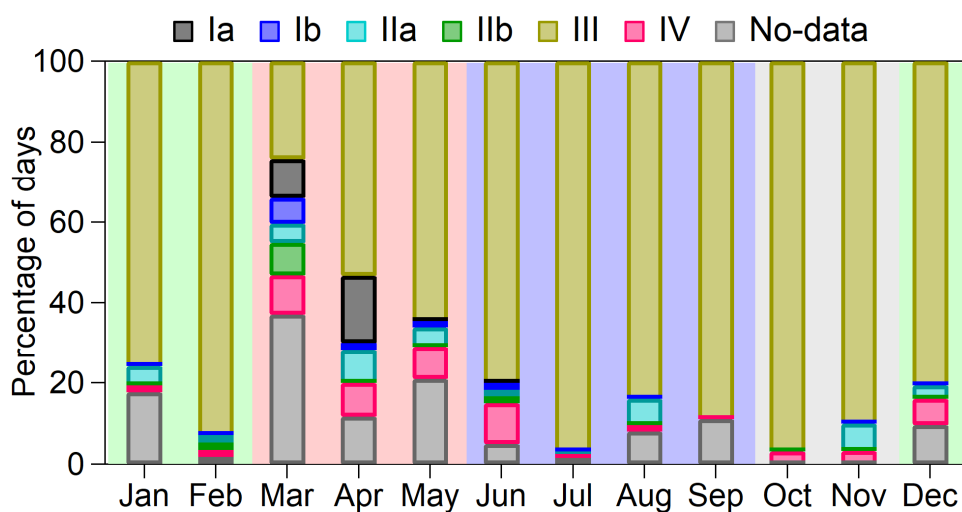


Figure 4. Monthly percentage of days for occurrence of NPF events (Ia, Ib, IIa, and IIb), non-event (III), unidentified (IV) and No-data days at Ranichauri. The background colours (light green, light red, light blue and light grey) indicate different seasons (winter, pre-monsoon, monsoon and post-monsoon, respectively).

3.2 Diurnal variation of aerosol parameters

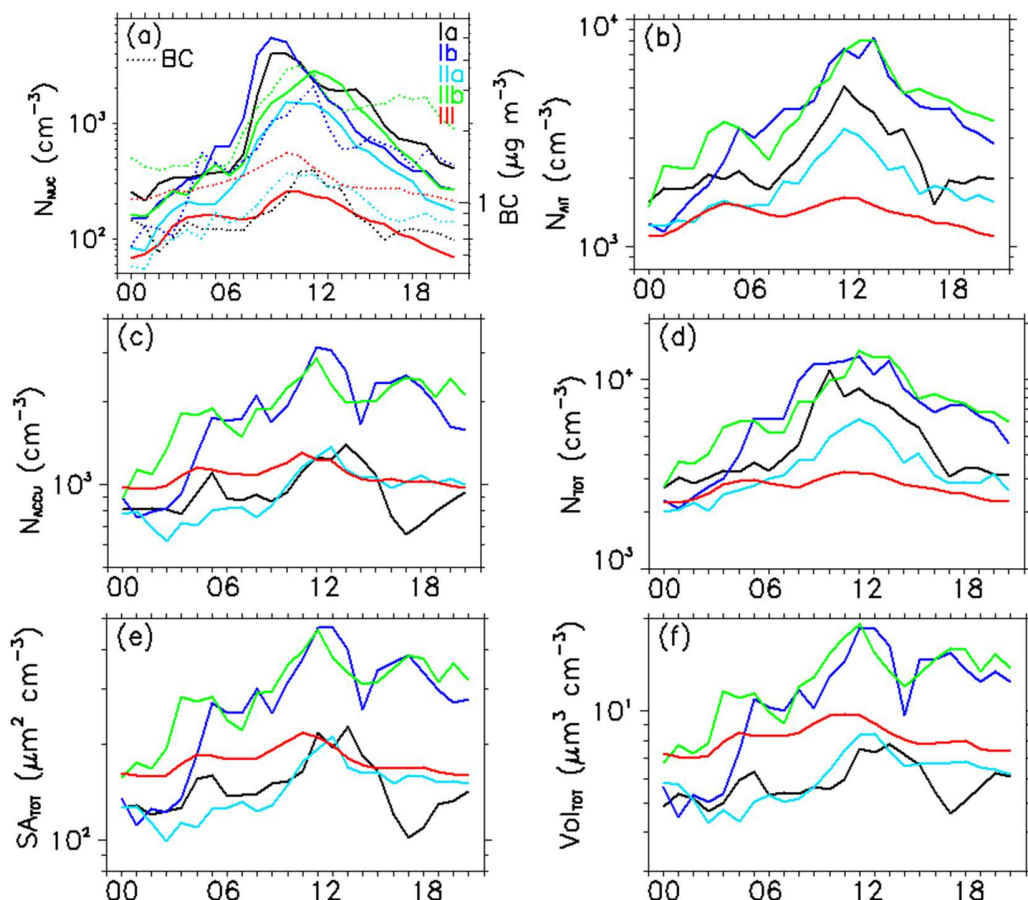
Figure 5 shows averaged diurnal variability in size-segregated aerosol number concentrations (Fig. 5a-d), BC mass concentration (dotted line, Fig. 5a), total surface area (Fig. 5e), total volume (Fig. 5f), total condensation sink (Fig. 5g), total coagulation sink (Fig. 5h), total mass (Fig. 5i) and particle mode diameter (Fig. 5j). Overall, we found two main types of diurnal variation patterns in aerosol concentrations and properties. The first type was clearly connected to NPF events, showing rapid diurnal changes in aerosol number concentrations and properties during mid-day. The second type was characterized as the background aerosol size distribution

and aerosol properties showing little or no diurnal change. These types of diurnal variation patterns are similar to previous studies reporting temporal evolution of aerosol number concentrations and properties from long-term ground-based measurements [Hooda *et al.*, 2018; Shen *et al.*, 2011; Venzac *et al.*, 2008]. We further describe these types below.

N_{NUC} has more than an order-of-magnitude diurnal variability on days with NPF events, but a factor of 2-3 on non-event days (Fig. 5a). The morning increase in N_{NUC} does not coincide with the increase in concentrations of anthropogenic aerosol tracer, indicated by BC for Type-Ia and Type-IIa cleaner events. However, the morning peak in N_{NUC} clearly coincides with the elevated BC concentrations for Type-Ib and Type-IIb polluted events (Fig. 5a). This is similar to observations at a high altitude site in the Western Himalaya reported by Venzac *et al.* [2008]. This finding is further corroborated by the presence of higher Aitken mode and accumulation mode concentrations for polluted events (Ib and IIb) than cleaner events (Ia and IIa) (Fig. 5g). The higher aerosol number concentrations on polluted days are also reflected in the diurnal variability in total surface area, total volume, total condensation sink, total coagulation sink, and total mass (Fig. 5d-i). In contrast, the particle mode diameter was smaller for cleaner event days than polluted event and non-event days (Fig. 5j). Similar diurnal variation of BC concentrations during Type-Ia, Type-IIa, and non-event days (Fig. 5a) perhaps illustrates that NPF was not prevented by the pre-existing aerosol concentrations in both cleaner and polluted air masses. In addition to pre-existing aerosol concentrations, there are two other factors that may strongly modulate NPF occurrence: availability of aerosol precursor concentration and solar insolation. At the high-altitude Hanle site in the Trans-Himalaya [Moorthy *et al.*, 2011], it was observed that NPF rates were higher during pre-monsoon as the solar insolation was abundant. In this study, NPF slowed as the seasons progressed towards winter. Neitola *et al.* [2011] reported frequent NPF at the Mukteshwar site in the North-Western Himalaya during the pre-monsoon season. They found that the high frequency of pre-monsoon events was linked to elevated boundary layer height, indicating availability of aerosol precursors transported from valley regions. A recent review study of ground-based high altitude sites indicated that the impact of CS on the occurrence of NPF appeared to be different from one high altitude site to another [Sellegrí *et al.*, 2019]. For instance, Venzac *et al.* [2008] found that high CS ($>2.1 \times 10^{-3} \text{ s}^{-1}$) inhibited the occurrence of NPF at the high-altitude Himalayan Nepal site, Pyramid, while the CS was higher during NPF events days ($3.1 \times 10^{-3} \text{ s}^{-1}$) than non-event days ($2.1 \times 10^{-3} \text{ s}^{-1}$) at the Mount

Chacaltaya site in Bolivian Andes [Rose *et al.*, 2015] (implying the opposite effect of condensation sink at Pyramid). Sellegrí *et al.* [2019] suggested that the occurrence of NPF at high altitude sites might be determined by the abundance of condensable vapors, which are transported together with pre-existing aerosols from lower altitudes. At Ranichauri, the NPF occurred at both low ($6.4 \times 10^{-3} \text{ s}^{-1}$) and high ($12.5 \times 10^{-3} \text{ s}^{-1}$) condensation sink conditions (Fig. 5g), with the ratio between polluted and cleaner event days of about 2.

Further, we have calculated averaged diurnal variation of meteorological parameters for observed Type-I, Type-II, and Type-III event days (Fig. S2). Temperature and relative humidity were slightly lower on non-event days as compared to event days. The wind direction rapidly changed on event days as compared to non-event days. Altogether, the meteorological parameters did not show much variation between the event and non-event days.



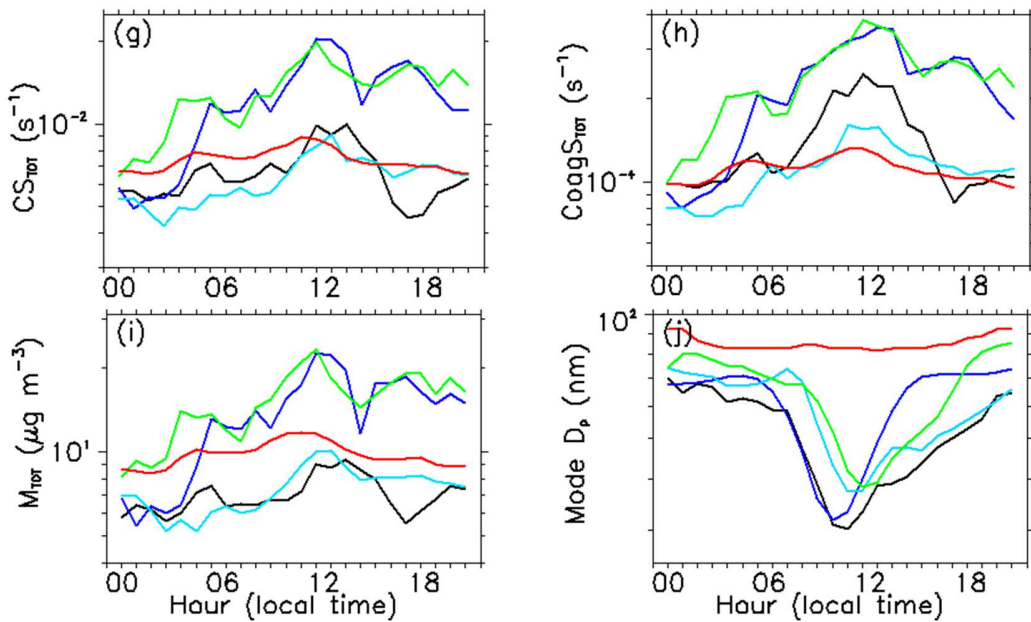


Figure 5. Averaged diurnal variation of (a) nucleation mode aerosols (solid lines) and black carbon mass concentrations (dotted line), (b) Aitken mode aerosols, (c) accumulation mode aerosols, (d) total aerosols, (e) total surface area, (f) total volume, (g) total condensation sink, (h) total coagulation sink, (i) total mass and (j) particle mode diameter for NPF (Type-I and -II) event and non-event (Type-III) days. Line colour indicates the type of event.

The occurrence of NPF events in different air mass types is another open question. Air masses of different origin pose not only different meteorological conditions, but also varying chemical features. Therefore, the probability of occurrence of NPF at a given location not only depends on local emissions, but also the type of air mass arriving at that location [Sogacheva *et al.*, 2005]. For instance, NPF events were more common in continental polluted air masses than that of cleaner marine air masses from the Atlantic Ocean [Hussein *et al.*, 2009; Sogacheva *et al.*, 2007]. Pierce *et al.* [2014] also showed that NPF rates were faster under the polluted conditions as compared to cleaner-air flow at Egbert, a mixture of forests and farmland site in Ontario, Canada. NPF has been seen to occur commonly at semi-rural and remote sites under the influence of long-range transported polluted plumes with elevated sulfuric acid concentrations via oxidation of sulfur dioxide [Creamean *et al.*, 2011; Kanawade *et al.*, 2012]. Neitola *et al.* [2011] showed that NPF occurs frequently in the pre-monsoon season at a high-altitude site, Mukteshwar in the Himalayan foot hills when the boundary layer height was lifted up to the

station altitude which allowed transport of aerosol precursors from valley to the station. These and numerous other studies found that NPF processes are strongly linked to the history of air masses [e.g. *Asmi et al.*, 2011; *Niemi et al.*, 2014; *Nilsson et al.*, 2001]. This is not surprising since air masses arriving from different locations are likely to be affected by varying concentrations of aerosol precursors and meteorological conditions prior to their arrival at the measurement site, which determines the age of the air mass.

Hyvärinen et al. [2010] used ratio of Aitken mode to Accumulation mode aerosols to determine the age of the air mass, where low values indicate an aged air mass while high values indicate the cleaner air mass often connected with NPF events. Figure 6 shows the hourly and monthly averaged ratio of Aitken mode to accumulation mode aerosols (N_{AIT}/N_{ACCU}) for NPF and non-event days. The site is dominated by Aitken mode aerosols almost throughout the year, with the highest ratios of N_{AIT} to N_{ACCU} during monsoon and pre-monsoon seasons. N_{AIT}/N_{ACCU} values are higher for non-event days than event days in the monsoon indicating the efficient wet scavenging of accumulation mode particles. N_{AIT}/N_{ACCU} values are higher for NPF event days than non-event days in the pre-monsoon season, indicating the large source of Aitken mode aerosols via NPF processes. The monthly mean ratio ranged from 1.5 to 4.2, with about 75% cleaner events (Ia and IIa) of total NPF events (Fig. 6).

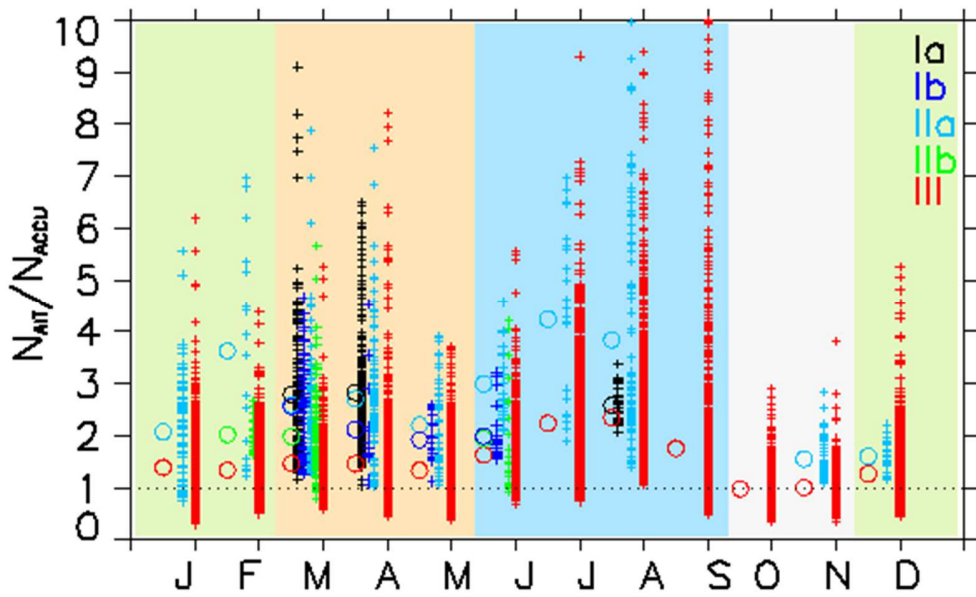


Figure 6. Hourly (plus sign) and monthly (open circle) averaged ratio of Aitken mode to accumulation mode aerosols for NPF event (Ia, Ib, IIa, and IIb) and non-event (III) days. The

background colours (light green, light red, light blue and light grey) indicate different seasons (winter, pre-monsoon, monsoon and post-monsoon, respectively).

3.3 Growth rate, formation rate and survival probabilities of climate-relevant aerosols

Growth rates, formation rates, and survival probabilities were calculated only for Type-Ia and Type-Ib event days. Table 2 summarizes mean, median, and percentile (25th and 75th) values for $GR_{10-25nm}$ and J_{10} for these event days. For Type-Ia events, the median $GR_{10-25nm}$ was 7.5 nm h⁻¹, with 6.2 and 11.2 nm h⁻¹ as 25th and 75th percentiles. For Type-Ib events, the median $GR_{10-25nm}$ was 4.2 nm h⁻¹, with 3.3 and 10.7 nm h⁻¹ as 25th and 75th percentiles. The mean $GR_{10-25nm}$ was 8.51 nm h⁻¹ and 4.86 nm h⁻¹ for Type-Ia and Type-Ib, respectively. Figure 7(a) illustrates the cumulative probability distribution functions for $GR_{10-25nm}$ for these event days. The particle growth rates were about two-fold higher for cleaner events than polluted events. This suggests that faster growth rates were favored at a lower condensation sink. Overall, $GR_{10-25nm}$ values are within the large range observed at other high altitude sites (0.4 to 19.9 nm h⁻¹) [Sellegrí *et al.*, 2019].

Table 2. Summary of particle growth and formation rates for Type-I event days. σ indicates standard deviation. p25 and p75 indicate 25th and 75th percentile values, respectively.

Event type	GR_{10-25} (nm h ⁻¹)		J_{10} (cm ⁻³ s ⁻¹)	
	Mean $\pm \sigma$	Median (p25-p75)	Mean $\pm \sigma$	Median (p25-p75)
Ia	8.51 \pm 4.46	7.53 (6.15 - 11.18)	0.26 \pm 0.27	0.21 (0.05 - 0.49)
Ib	4.86 \pm 3.13	4.17 (3.29 - 10.71)	0.09 \pm 0.08	0.07 (0.02 - 0.19)

The mean J_{10} was 0.26 cm⁻³ s⁻¹ and 0.09 cm⁻³ s⁻¹ for Type-Ia and Type-Ib events, respectively. For Type-Ia event days, the median J_{10} was 0.21 cm⁻³ s⁻¹, with 0.05 and 0.49 cm⁻³ s⁻¹ as 25th and 75th percentile values whereas for Type-Ib events, median J_{10} was 0.07 cm⁻³ s⁻¹, with 0.02 and 0.19 cm⁻³ s⁻¹ as 25th and 75th quartile values. Figure 7(b) illustrates the cumulative probability distribution functions for J_{10} for these event days. García *et al.* [2014] reported J_{10} , at a high-altitude Izaña station in the Atlantic Ocean, in the range from 0.5 - 0.6 cm⁻³ s⁻¹ whereas

[Venzac *et al.*, 2008] reported, at a high altitude NCO-P site, in the range from 0.1 - 0.2 $\text{cm}^{-3} \text{ s}^{-1}$. J_{10} at Ranichauri is comparable to these values, and to one reported for the Mukteshwar site in the Himalayan foothills ($0.4 \text{ cm}^{-3} \text{ s}^{-1}$) [Neitola *et al.*, 2011]. Nevertheless, J_{10} values at Ranichauri falls within the wide range reported for high-altitude and continental boundary layer sites across the globe ($0.01 - 10 \text{ cm}^{-3} \text{ s}^{-1}$) [Kulmala *et al.*, 2004; Sellegrí *et al.*, 2019].

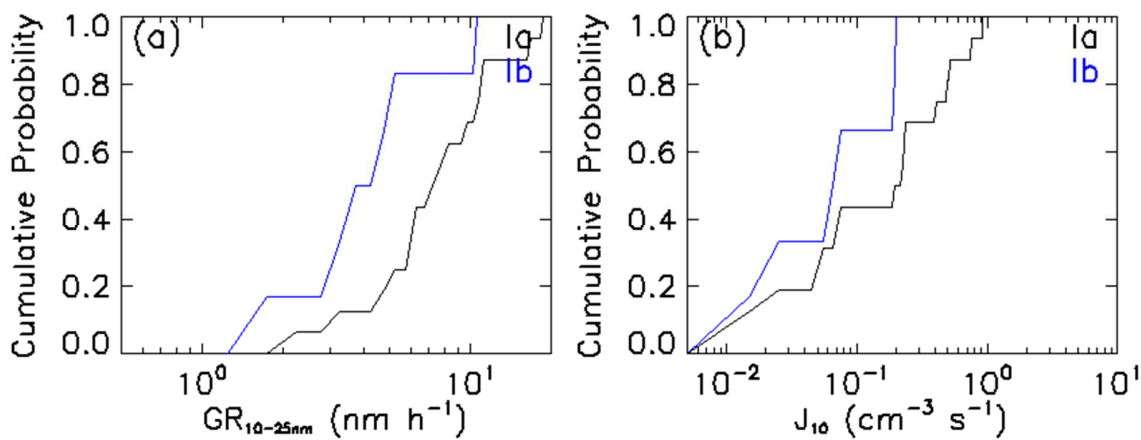


Figure 7. Cumulative probability distributions of (a) $\text{GR}_{10-25\text{nm}}$ and (b) J_{10} for Type-Ia and -Ib NPF event days.

The contribution of atmospheric NPF to total aerosols or CCN concentrations can be estimated from the aerosol size distribution data. Kulmala *et al.* [2016a] estimated that NPF contributes about 80% to the total aerosol number concentrations in a rural forest site, SMEAR II station at Hyytiälä, Finland. But, Tröstl *et al.* [2016] highlighted, based on 12-month aerosol size distribution data from the high-altitude site, Jungfraujoch, that NPF adds about 10% new particles to the aerosol concentration below 50 nm. They further emphasized that newly formed particles do not grow to CCN-active size (for an activation diameter of $\sim 90 \text{ nm}$ [Jurányi *et al.*, 2011]) within observed NPF time-scales at this site (48 hours), yielding low contribution of NPF to the CCN concentrations. The measurements at Mt. Tai in Shandong Province in China also showed that only about 12% of the total NPF events showed enhancement in CCN concentrations [Shen *et al.*, 2016]. There is also no direct evidence of NPF contribution to CCN size at other high altitude sites e.g. NCO-Pyramid, Chacaltaya or Storm Peak Laboratory [Hallaar *et al.*, 2016; Rose *et al.*, 2015; Venzac *et al.*, 2008]. Additionally, observations at Whistler Mountain ($\sim 1300 \text{ m amsl}$) showed that freshly nucleated particles had a 10 - 25% probability of

growing to CCN sizes (100 nm) before being scavenged by coagulation [Pierce *et al.*, 2012] whereas aerosol size distribution data at Chacaltaya mountain found that the potential to form CCN was about 53% in the free troposphere [Rose *et al.*, 2017]. Further, sulfuric acid is the dominant contributor to initial growth of nanoparticles from NPF, while organic compounds become more important as particles grow larger [Kulmala *et al.*, 2016b]. Thus, the growth of nucleated particles to CCN sizes is dependent on the source and chemical makeups of the precursor compounds [Wang *et al.*, 2017] as well as sinks (such as coagulations to pre-existing particles) [Kulmala *et al.*, 2005]. Since the growth of nucleated particles to CCN sizes takes from a few hours up to about three days in the lower troposphere, it is observationally very challenging to distinguish CCN formed through atmospheric NPF from those formed from growth of pre-existing aerosols [Kerminen *et al.*, 2012].

Figure 8 shows cumulative probability distribution functions for the survival probability to 50 nm and 100 nm particles (SP50 and SP100) and the formation rates of 50 nm and 100 nm particles (J_{50} and J_{100}) for Type-I events. Table 3 summarizes survival probabilities (SP) and formation rates (J) of 50 nm and 100 nm particles from various sites across the globe. SP50 ranged from 44% to 98%, with a mean and standard deviation of $82 \pm 18\%$ and SP100 ranged from 5% to 94%, with a mean and standard deviation of $53 \pm 32\%$. These results show that, on average, 64% of new particle surviving to 50 nm goes on to survive to 100 nm. With the observed mean particle growth rates of 8.51 nm h^{-1} , the newly formed particles survived approximately 4 to 6 hours to reach 50 nm. The mean value of SP50 at Ranichauri is almost double of the value reported for low-altitude forest site (33%) [Pierce *et al.*, 2014] and comparable to the observed range at all four urban sites (31-80%) reported by Westervelt *et al.* [2013]. There are uncertainties in calculation of survival probabilities to 50 nm and 100 nm particles as previously reported by Westervelt *et al.* [2013]. First, the primary particles may contribute to particle number concentrations of 10 to 25 nm, and therefore contributing to the apparent nucleation rate. The use of two growth rates for only two size ranges (10-25 nm and 25-100 nm) may bias survival probabilities higher than expected. But, Westervelt *et al.* [2013] quantitatively addressed the survival probability uncertainty by using two methods: one method identified in the paper, and the other described by Kuang *et al.* [2009], wherein the ratio of N_{100} to N_3 for a given growth trajectory is defined as the survival probability. Westervelt *et al.* [2013] found that the two methods largely yield similar survival probabilities. J_{50} and J_{100} are the

products of J_{10} and the corresponding survival probabilities. J_{50} ranged from 0.009 to $0.17 \text{ cm}^{-3} \text{ s}^{-1}$, with a mean and standard deviation of $0.08 \pm 0.05 \text{ cm}^{-3} \text{ s}^{-1}$, which is about two times higher than a low altitude site in Egbert, Ontario, Canada [Pierce *et al.*, 2014] where J_{50} was $0.039 \text{ cm}^{-3} \text{ s}^{-1}$ and lower by almost one-fifth to that of a highly polluted site, Po Valley ($0.39 \text{ cm}^{-3} \text{ s}^{-1}$) [Westervelt *et al.*, 2013]. J_{100} ranged from 0.004 to $0.16 \text{ cm}^{-3} \text{ s}^{-1}$, with a mean and standard deviation of $0.05 \pm 0.04 \text{ cm}^{-3} \text{ s}^{-1}$, which is about 2-3 times higher than low altitude site, Egbert, Ontario, Canada ($0.02 \text{ cm}^{-3} \text{ s}^{-1}$) [Pierce *et al.*, 2014]. While J_{100} at Ranichauri was lower by an order of magnitude than that at the Po Valley ($0.34 \text{ cm}^{-3} \text{ s}^{-1}$) [Westervelt *et al.*, 2013]. The ratio of J_{100} to J_{50} ranged from 0.10 to 0.99, with a mean value of about 0.60 ± 0.31 .

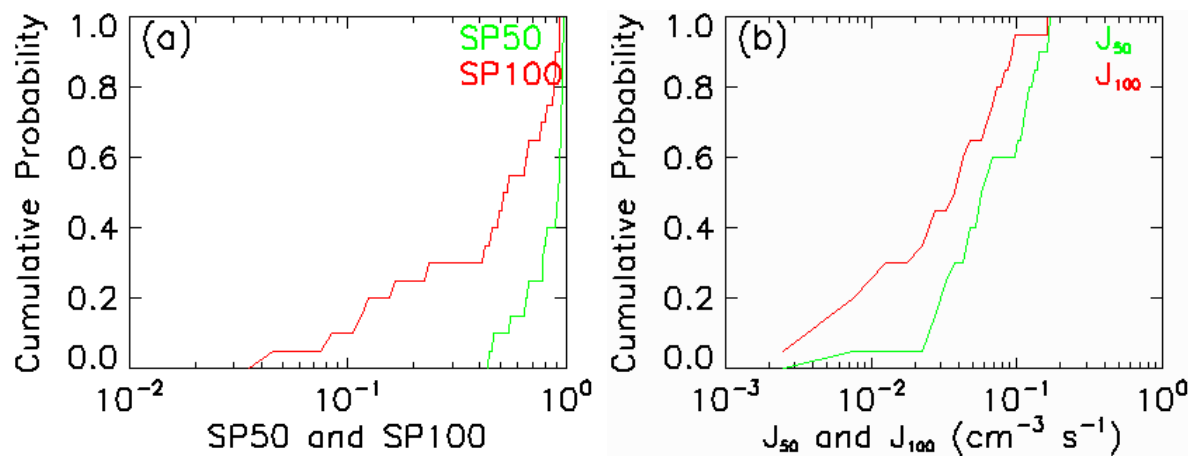


Figure 8. Cumulative probability distributions of (a) survival probability to 50 nm and 100 nm and (b) formation rates of 50 nm and 100 nm particles for the Type-I events.

Table 3. Summary of survival probability and formation rate of 50 nm and 100 nm particles at diverse locations.

Location	SP50 (%)	SP100 (%)	J_{50} (cm ⁻³ s ⁻¹)	J_{100} (cm ⁻³ s ⁻¹)	Reference
Ranichauri, India	82 ± 18	53 ± 32	0.08 ± 0.05	0.05 ± 0.04	This study
Egbert, Ontario, Canada	33	19	0.039	0.022	Pierce <i>et al.</i> [2014]
Pittsburgh, USA	37	2.4	0.11	0.006	Westervelt <i>et al.</i> [2013]
Atlanta, USA	67	3.7	0.177	0.006	Westervelt <i>et al.</i> [2013]
St. Louis, USA	46	1.8	1.6	0.046	Westervelt <i>et al.</i> [2013]
Hyytiälä, Finalnd	55	2.6	0.23	0.004	Westervelt <i>et al.</i> [2013]
Po Valley, Itlay	34	4.4	0.39	0.34	Westervelt <i>et al.</i> [2013]
Mt. Tai, China	10-140	5-40	-	-	[Zhu <i>et al.</i> , 2020]

While the size of aerosol particle determines its ability to act as CCN, the hygroscopicity of particle also affects CCN activation [McFiggans *et al.*, 2006]. Figure 9 shows relative (in %) and absolute (in cm^{-3}) increase in CCN concentrations for Type-I nucleation event days at Ranichauri. Analogous to SP50 and SP100 calculations, nucleation events had an obvious effect on CCN concentrations. The relative increase in N_{50} ranged from 21.6 to 577.1 %, with a mean and standard deviation of 247 ± 198 % whereas the absolute increase in N_{50} ranged from 541 to 7964 cm^{-3} , with a mean and standard deviation of $3631 \pm 2603 \text{ cm}^{-3}$. The absolute increase in N_{50} at Ranichauri is comparable to continental background site, Botsalano, South Africa [Kerminen *et al.*, 2012], indicative of intense nucleation events with higher growth rates. The relative increase in N_{100} ranged from 17.8 to 579.4 %, with a mean and standard deviation of 201 ± 165 % whereas the absolute increase in N_{100} ranged from 211 to 2451 cm^{-3} , with a mean and standard deviation of $1290 \pm 913 \text{ cm}^{-3}$.

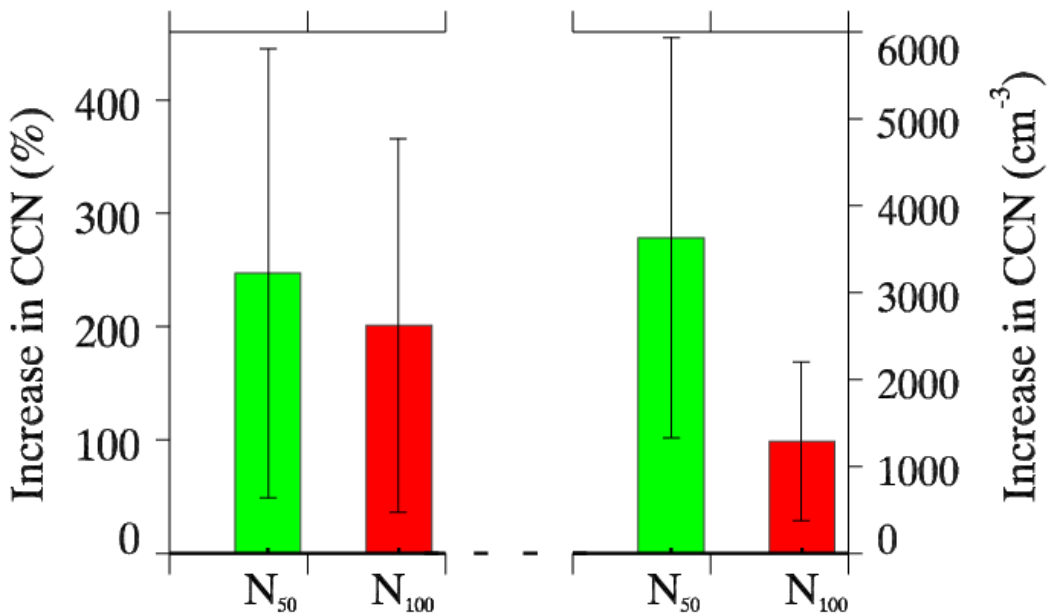


Figure 9. The relative (%) and absolute (cm^{-3}) increase in CCN concentrations during Type-I NPF event days.

4. Conclusions

Here, we presented aerosol size distribution measurements at a background remote site, Ranichauri based on a 21-months (1 December 2016 to 14 September 2018). We reported the frequency of NPF occurrence, growth rate, formation rate, seasonal variability and diurnal patterns in NPF features and illustrated survival probability of newly formed aerosols to 50 nm and 100 nm particles. Out of 643 observation days, Type-I (clear NPF events) and Type-II NPF (Aitken-mode growth) events were observed on 3.6% and 4.8% days, respectively, with highest NPF frequency in the pre-monsoon (March-May) season. Type-I and Type-II NPF events were further classified into two sub-types: a (cleaner) and b (polluted), based on BC mass concentrations. For Type-Ia NPF event days, the $\text{GR}_{10-25\text{nm}}$ varied from 2.1 to 18.5 nm h^{-1} , with a mean and standard deviation of $8.51 \pm 4.46 \text{ nm h}^{-1}$ and for Type-Ib events, it varied from 1.6 to 10.7 nm h^{-1} with mean and standard deviation of $4.86 \pm 3.13 \text{ nm h}^{-1}$. For Type-Ia events, J_{10} varied from 0.01 to $0.91 \text{ cm}^{-3} \text{ s}^{-1}$ with a mean and standard deviation of $0.26 \pm 0.27 \text{ cm}^{-3} \text{ s}^{-1}$, whereas it varied from 0.01 to $0.24 \text{ cm}^{-3} \text{ s}^{-1}$ with mean and standard deviation of $0.09 \pm 0.08 \text{ cm}^{-3} \text{ s}^{-1}$.

Accepted Article

s^{-1} for Ib event days. The newly formed particle survival probability to 50 nm size ranged from 44 to 98%, with a mean and standard deviation of $82 \pm 18\%$, and the survival probability to 100 nm was $53 \pm 32\%$. Our estimates of survival probability indicate that a significant fraction of nucleated particles grow larger than 50 nm and 100 nm, and thus constitute an important source of CCN for cloud formations. The uplifting of the planetary boundary layer to the elevation of the measurement site appeared to carry aerosol precursor vapors for particle growth at a relatively lower background pre-existing particle concentrations. The mean formation rates of 50 nm and 100 nm particles were $0.08 \text{ cm}^{-3} \text{ s}^{-1}$ and $0.05 \text{ cm}^{-3} \text{ s}^{-1}$, respectively. The newly formed particles have an obvious effect on CCN number concentrations during the observed NPF event days. Overall, NPF occurred more frequently in air masses with low BC concentrations (cleaner) than polluted air masses, with faster growth rates and formation rates during cleaner event days (Type-Ia). While the high condensation sink in polluted air masses could reduce the concentrations of condensable vapors and in turn lowering NPF and growth rates, the chemistry producing condensable vapors may also significantly alter NPF and growth rates. Our results highlight that although the occurrence of NPF was lower at this site as compared to other remote high altitude sites, the high survival probability indicates that the sporadic NPF events could be a large source of climate-relevant aerosols.

In this study, we have linked, for the first time to our knowledge, NPF to climate-relevant aerosols in India. First, more emphasis should be put on combining long-term field measurements from multiple sites in India to derive statistically relevant NPF features including frequency, growth rates, formation rates, survival probability of newly formed aerosols, and CCN concentrations or some proxy for it. Second, adding chemical information and CCN concentration measurements to the existing aerosol size distribution measurements would provide new information on NPF-CCN linkages in cleaner versus polluted environments. Lastly, such analyses of field measurements should be aided with regional or parcel model simulations to aid in interpreting field measurements.

Acknowledgments and Data Availability

V. P. Kanawade would like to thank Department of Science & Technology (DST)-SERB Grant (ECR/2016/001333). CLIMOB (CLImate Modelling and Observations in India) - project

funded by the Ministry for Foreign Affairs of Finland is acknowledged for supporting the measurements in Ranichauri. J. R. Pierce was supported by the US Department of Energy's Atmospheric System Research, an Office of Science, Office of Biological and Environmental Research program, under grant DE-SC0019000. Authors acknowledge the free use of PC-based HYSPLIT model. Authors also thank the anonymous reviewers for their many insightful comments and suggestions which helped to improve the quality of the manuscript.

DMPS aerosol size distribution and AE-33 Aethelometer black carbon data are archived at <https://data.mendeley.com/datasets/pstmtr8gzs/2>. Air mass back trajectory calculation is performed using PC windows-based HYSPLIT model, which is available publicly at <https://www.ready.noaa.gov/HYSPLIT.php>.

References

- Asmi, E., N. Kivekäs, Kerminen, V.-M., Komppula, M., Hyvärinen, A. P., Hatakka, J., Viisanen, Y., & Lihavainen H. (2011). Secondary new particle formation in Northern Finland Pallas site between the years 2000 and 2010. *Atmospheric Chemistry and Physics*, 11(24), 12959-12972. <https://doi.org/10.5194/acp-11-12959-2011>
- Babu, S. S., Kompalli, S. K., & Moorthy K. K. (2016). Aerosol number size distributions over a coastal semi urban location: Seasonal changes & ultrafine particle bursts. *Science of The Total Environment*, 563–564, 351-365. <https://doi.org/10.1016/j.scitotenv.2016.03.246>
- Boulon, J., Sellegrí, K., Venzac, H., D. Picard, D., Weingartner, E., Wehrle, G., Coen, M. C., Bütikofer, R., Flückiger, E., Baltensperger, U., & Laj, P. (2010). New particle formation and ultrafine charged aerosol climatology at a high altitude site in the Alps (Jungfraujoch, 3580 m a.s.l., Switzerland). *Atmospheric Chemistry and Physics*, 10(19), 9333-9349. <https://doi.org/10.5194/acp-10-9333-2010>
- Chowdhury, S., Dey, S., & Smith, K. R. (2018). Ambient PM_{2.5} exposure and expected premature mortality to 2100 in India under climate change scenarios. *Nature Communications*, 9(1), 318. <https://doi.org/10.1038/s41467-017-02755-y>
- Collaud Coen, M., et al. (2013), Aerosol decadal trends – Part 1: In-situ optical measurements at GAW and IMPROVE stations, *Atmospheric Chemistry and Physics*, 13(2), 869-894.
- Creamean, J. M., Ault, A. P., Hoeve, J. E. T., Jacobson, M. Z., Roberts, G. C., & Prather, K. A. (2011). Measurements of Aerosol Chemistry during New Particle Formation Events at a Remote Rural Mountain Site. *Environmental Science & Technology*, 45(19), 8208-8216. <https://doi.org/10.1021/es103692f>

Dai, L., Wang, H., Zhou, L., An, J., Tang, L., Lu, C., Yan, W., Liu, R., Kong, S., Chen, M., Lee, S-H., & Yu, H. (2017). Regional and local new particle formation events observed in the Yangtze River Delta region, China. *Journal of Geophysical Research: Atmospheres*, 122(4), 2389-2402. <https://doi.org/10.1002/2016JD026030>

Dal Maso, M. D., Kulmala, M., Riipinen, I., Wagner, R., Hussein, T., Aalto, P. P., & Lehtinen, K. E. J. (2005). Formation and growth of fresh atmospheric aerosols: eight years of aerosol size distribution data from SMEAR II, Hyytiälä, Finland. *Boreal Environment Research*, 10(5), 323-336.

De Wekker, S. F. J., and M. Kossman (2015), Convective Boundary Layer Heights Over Mountainous Terrain—A Review of Concepts, *Frontiers in Earth Science*, 3(77).

Draxler, R. R., & G. D. Rolph (2010). HYSPLIT—HYbrid Single-Particle Lagrangian Integrated Trajectory Model. Available online: <http://ready.arl.noaa.gov/HYSPLIT.php>.

Drinovec, L., Močnik, G., Zotter, P., Prévôt, A. S. H., Ruckstuhl, C., Coz E., Rupakheti, M., Sciare, J., Müller, T., Wiedensohler, A., & Hansen, A. D. A. (2015). The "dual-spot" Aethalometer: an improved measurement of aerosol black carbon with real-time loading compensation. *Atmospheric Measurement Techniques*, 8(5), 1965-1979. <https://doi.org/10.5194/amt-8-1965-2015>

Dusek, U., Frank, G. P., Hildebrandt, L., Curtius, J., Schneider, J., Walter, S., Chand, D., Drewnick, F., Hings, S., Jung, D., Borrmann, S., & Andreae, M. O. (2006). Size Matters More Than Chemistry for Cloud-Nucleating Ability of Aerosol Particles. *Science*, 312(5778), 1375-1378. <https://doi.org/10.1126/science.1125261>

Foucart, B., Sellegrí, K., Tulet, P., Rose, C., Metzger, J. M., & Picard, D. (2018). High occurrence of new particle formation events at the Maïdo high-altitude observatory (2150 m), Réunion (Indian Ocean). *Atmospheric Chemistry and Physics*, 18(13), 9243-9261. <https://doi.org/10.5194/acp-18-9243-2018>

García, M. I., Rodríguez, S., González, Y., & García, R. D. (2014). Climatology of new particle formation at Izaña mountain GAW observatory in the subtropical North Atlantic. *Atmospheric Chemistry and Physics*, 14(8), 3865-3881. <https://doi.org/10.5194/acp-14-3865-2014>

Gordon, H., Kirkby, J., Baltensperger, U., Bianchi, F., Breitenlechner, M., Curtius, J., Dias, A., Dommen, J., Donahue, N. M., Dunne, E. M., Duplissy, J., Ehrhart, S., Flagan, R. C., Frege, C., Fuchs, C., Hansel, A., Hoyle C. R., Kulmala, M., Kürten, A., Lehtipalo, K., Makhmutov, V., Molteni, U., Rissanen, M. P., Stozkhov, Y., Tröstl, J., Tsagkogeorgas, G., Wagner, R., Williamson, C., Wimmer, D., Winkler, P. M., Yan, C., & Carslaw, K. S. (2017). Causes and importance of new particle formation in the present-day and preindustrial atmospheres. *Journal of Geophysical Research: Atmospheres*, 122(16), 8739-8760. <https://doi.org/10.1002/2017JD026844>

Hallar, A. G., Lowenthal, D. H., Chirokova, G., Borys, R. D., & Wiedinmyer, C. (2011). Persistent daily new particle formation at a mountain-top location. *Atmospheric Environment*, 45(24), 4111-4115. <https://doi.org/10.1016/j.atmosenv.2011.04.044>

Hallar, A. G., Petersen, R., McCubbin, I. B., Lowenthal, D., Lee, S-H., Andrews E., & Yu F. (2016). Climatology of New Particle Formation and Corresponding Precursors at Storm Peak Laboratory, *Aerosol and Air Quality Research*, 16(3), 816-826.
<https://doi.org/10.4209/aaqr.2015.05.0341>

Hooda, R. K., Kivekäs, N., O'Connor, E. J., Collaud Coen, M., Pietikäinen, J.-P., Vakkari, V., Backman, J., Henriksson, S. V., Asmi, E., Komppula, M., Korhonen, H., Hyvärinen, A.-P., & Lihavainen, H., (2018). Driving Factors of Aerosol Properties Over the Foothills of Central Himalayas Based on 8.5 Years Continuous Measurements. *Journal of Geophysical Research: Atmospheres*, 123(23), 13,421-13,442. <https://doi.org/10.1029/2018JD029744>

Hussein, T., Junninen, H., Tunved, P., Kristensson, A., Maso, M. D., Riipinen, I., Aalto, P. P., Hansson, H. C., Swietlicki, E., & Kulmala, M. (2009), Time span and spatial scale of regional new particle formation events over Finland and Southern Sweden. *Atmospheric Chemistry and Physics*, 9(14), 4699-4716. <https://doi.org/10.5194/acp-9-4699-2009>

Hyvärinen, A.-P., Lihavainen, H., Komppula, M., Panwar, T. S., Sharma, V. P., Hooda, R. K., & Viisanen, Y. (2010). Aerosol measurements at the Gual Pahari EUCAARI station: preliminary results from in-situ measurements. *Atmospheric Chemistry and Physics*, 10(15), 7241-7252.
<https://doi.org/10.5194/acp-10-7241-2010>

Hyvärinen, A.-P., Raatikainen, T., Komppula, M., Mielonen, T., Sundström, A.-M., Brus, D., Panwar, T. S., Hooda, R. K., Sharma, V. P., de Leeuw G., & Lihavainen H. (2011). Effect of the summer monsoon on aerosols at two measurement stations in Northern India – Part 2: Physical and optical properties. *Atmospheric Chemistry and Physics*, 11(16), 8283-8294.
<https://doi.org/10.5194/acp-11-8283-2011>

IPCC (2013), Climate Change 2013: The Physical Science Basis. Contribution of Working Group I to the Fifth Assessment Report of the Intergovernmental Panel on Climate Change Rep., 1535 pp. pp, Cambridge, United Kingdom and New York, NY, USA, .
<https://www.ipcc.ch/report/ar5/wg1/>

Jurányi, Z., Gysel, M., Weingartner, E., Bukowiecki, N., Kammermann, L., & Baltensperger, U. (2011). A 17 month climatology of the cloud condensation nuclei number concentration at the high alpine site Jungfraujoch. *Journal of Geophysical Research: Atmospheres*, 116(D10).
<https://doi.org/10.1029/2010JD015199>

Kamra, A. K., Siinigh, D., Gautam, A. S., Kanawade, V. P., Tripathi, S. N., & Srivastava, A. K. (2015). Atmospheric ions and new particle formation events at a tropical location, Pune, India, *Quarterly Journal of the Royal Meteorological Society*, 141(693), 3140-3156.
<https://doi.org/10.1002/qj.2598>

Kanamitsu, M. (1989), Description of the NMC Global Data Assimilation and Forecast System. *Weather and Forecasting*, 4(3), 335-342.

Kanawade, V. P., Benson, D. R., & Lee, S.-H. (2012), Statistical analysis of 4-year observations of aerosol sizes in a semi-rural continental environment, *Atmospheric Environment*, 59, 30-38.
<http://dx.doi.org/10.1016/j.atmosenv.2012.05.047>

Kanawade, V. P., Tripathi, S. N., Chakraborty, A., & Yu, H. (2020), Chemical Characterisation of Sub-micron Aerosols During New Particle Formation in an Urban Atmosphere, *Aerosol and Air Quality Research* 20, 1294–1305.. <https://doi.org/10.4209/aaqr.2019.04.0196>

Kanawade, V. P., Tripathi, S. N., Siingh, D., Gautam, A. S., Srivastava, A. K., Kamra, A. K., Soni, V. K., and Sethi, V. (2014a). Observations of new particle formation at two distinct Indian subcontinental urban locations. *Atmospheric Environment*, 96, 370-379. <http://dx.doi.org/10.1016/j.atmosenv.2014.08.001>

Kanawade, V.P., Shika, S., Pöhlker, C., Rose, D., Suman, M. N. S., Gadhavi, H., Kumar, A., Nagendra, S. M. S., Ravikrishna, R., Yu, H., Sahu, L.K., Jayaraman, A., Andreae, M.O., Pöschl, U., & Gunthe, S.S. (2014b). Infrequent occurrence of new particle formation at a semi-rural location, Gadanki, in tropical Southern India, *Atmospheric Environment*, 94, 264-273. <http://dx.doi.org/10.1016/j.atmosenv.2014.05.046>

Kerminen, V.-M., Chen, X., Vakkari, V., Petäjä, T., Kulmala, M., & Bianchi, F. (2018). Atmospheric new particle formation and growth: review of field observations. *Environmental Research Letters*, 13(10), 103003. <https://doi.org/10.1088/1748-9326/aadf3c>

Kerminen V.-M., Paramonov, M., Anttila, T., Riipinen, I., Fountoukis, C., Korhonen, H., Asmi, E., Laakso, L., Lihavainen, H., Swietlicki, E., Svenningsson, B., Asmi, A., Pandis S. N., Kulmala M., & Petäjä, T. (2012). Cloud condensation nuclei production associated with atmospheric nucleation: a synthesis based on existing literature and new results. *Atmospheric Chemistry and Physics*, 12(24), 12037-12059. <https://doi.org/10.5194/acp-12-12037-2012>

Kivekäs, N., Sun, J., Zhan, M., Kerminen, V.-M., Hyvärinen, A., Komppula, M., Viisanen, Y., Hong, N., Zhang, Y., Kulmala, M., Zhang, X.-C., Deli-Geer, & Lihavainen, H. (2009), Long term particle size distribution measurements at Mount Waliguan, a high-altitude site in inland China. *Atmospheric Chemistry and Physics*, 9(15), 5461-5474. <https://doi.org/10.5194/acp-9-5461-2009>

Komppula, M., Lihavainen, H., Hyvärinen, A. P., Kerminen, V.-M., Panwar, T. S., Sharma, V. P., & Viisanen, Y. (2009). Physical properties of aerosol particles at a Himalayan background site in India. *Journal of Geophysical Research: Atmospheres*, 114(D12). <https://doi.org/10.1029/2008JD011007>

Korhonen, H., K. S. Carslaw, D. V. Spracklen, D. A. Ridley, and J. Ström (2008), A global model study of processes controlling aerosol size distributions in the Arctic spring and summer, *Journal of Geophysical Research: Atmospheres*, 113(D8).

Kowol-Santen, J., M. Beekmann, S. Schmitgen, and K. Dewey (2001), Tracer analysis of transport from the boundary layer to the free troposphere, *Geophysical Research Letters*, 28(15), 2907-2910.

Kuang, C., McMurry P. H., & McCormick A. V. (2009). Determination of cloud condensation nuclei production from measured new particle formation events, *Geophysical Research Letters*, 36(9), n/a-n/a. <https://doi.org/10.1029/2009GL037584>

Kulmala, M., Kerminen, V. M., Petäjä, T., Ding, A. J., & Wang, L. (2017). Atmospheric gas-to-particle conversion: why NPF events are observed in megacities?, *Faraday Discussions*, 200(0), 271-288. <https://doi.org/10.1039/c6fd00257a>

Kulmala, M., Vehkamäki, H., Petäjä, T., Maso, M. D., Lauri, A., Kerminen, V.-M., Birmili, W., and McMurry, P. H. (2004). Formation and growth rates of ultrafine atmospheric particles: a review of observations. *Journal of Aerosol Science*, 35(2), 143-176. <https://doi.org/10.1016/j.jaerosci.2003.10.003>

Kulmala, M., T. Petäjä, P. Mönkkönen, I. K. Koponen, M. Dal Maso, P. P. Aalto, K. E. J. Lehtinen, and V. M. Kerminen (2005), On the growth of nucleation mode particles: source rates of condensable vapor in polluted and clean environments, *Atmospheric Chemistry and Physics*, 5(2), 409-416. <https://doi.org/10.5194/acp-5-409-2005>

Kulmala, M., Luoma, K., Virkkula, A., Petäjä, T., Paasonen, P., Kerminen, V.-M., Nie, W., Qi, X., Shen, Y., Chi, X., & Ding, A. (2016a). On the mode-segregated aerosol particle number concentration load: contributions of primary and secondary particles in Hyytiälä and Nanjing. *Boreal Environment Research.*, 21(3-4), 319–331.

Kulmala, M., Petäjä, T., Kerminen, V.-M., Kujansuu, J., Ruuskanen, T., Ding, A., Nie, W., Hu, M., Wang, Z., Wu, Z., Wang, L. & Worsnop, D. R. (2016b). On secondary new particle formation in China, *Frontiers of Environmental Science & Engineering*, 10(5), 8.

Kulmala , M., Kontkanen, J., Junninen, H., Lehtipalo, K., Manninen, H. E., Nieminen, T., Petäjä, T., Sipilä, M., Schobesberger, S., Rantala, P., Franchin, A., Jokinen, T., Järvinen, E., Äijälä, M., Kangasluoma, J., Hakala, J., Aalto, P. P., Paasonen, P., Mikkilä, J., Vanhanen, J., Aalto, J., Hakola, H., Makkonen, U., Ruuskanen, T., Mauldin 3rd, R. L., Duplissy, J., Vehkamäki, V., Bäck, J., Kortelainen, A., Riipinen, I., Kurtén, T., Johnston, M. V., Smith, J. N., Ehn, M., Mentel, T. F., Lehtinen, K. E. J., Laaksonen, A., Kerminen, V.-M., Worsnop, D.R., (2013). Direct Observations of Atmospheric Aerosol Nucleation. *Science*, 339(6122), 943-946. <https://doi.org/10.1126/science.1227385>

Kumar, R. R., Soni, V. K., & Jain, M. K. (2020). Evaluation of spatial and temporal heterogeneity of black carbon aerosol mass concentration over India using three year measurements from IMD BC observation network. *Science of The Total Environment*, 723, 138060. <https://doi.org/10.1016/j.scitotenv.2020.138060>

Landrigan, P. J., Fuller, R., Acosta, N. J. R., Adeyi, O., Arnold , R., Basu, N. N., Baldé , A. B., Bertollini, R., Bose-O'Reilly, S., Boufford, J. I. , Breysse , P. N., Chiles , T., Mahidol , C., Coll-Seck, A. M., Cropper , M., Fobil , J., Fuster, V., Greenstone, M., Haines, A., Hanrahan, D., Hunter, D., Khare, M., Krupnick, A., Lanphear, B., Lohani, B., Martin, K., Mathiasen, K. V., McTeer, M. A., Murray, C. J. L., Ndahimamanjara, J.D., Perera, F., Potočnik, J., Preker, A. S., Ramesh, J., Rockström, J., Salinas, C., Samson, L. D. , Sandilya, K., Sly, P. D., Smith, K. R., Steiner, A., Stewart, R. B. , Suk, W. A., van Schayck, O. C. P., Yadama, G. N., Yumkella, K., & Zhong, M. (2018). The Lancet Commission on pollution and health. *The Lancet*. 391(10119), 462-512. [https://doi.org/10.1016/S0140-6736\(17\)32345-0](https://doi.org/10.1016/S0140-6736(17)32345-0)

Leaitch, W. R., Korolev, A., Aliabadi, A. A., Burkart, J., Willis, M. D., Abbatt, J. P. D., Bozem, H., Hoor, P., Köllner, F., Schneider, J., Herber, A., Konrad, C. and Brauner, R. (2016), Effects of 20-100 nm particles on liquid clouds in the clean summertime Arctic, *Atmospheric Chemistry and Physics*, 16(17), 11107-11124, doi: <https://doi.org/10.5194/acp-16-11107-2016>

Leena, P. P., Kumar V. A., Dani K. K., Sombawne S. M., Murugavel P., & Pandithurai G. (2017). Evidence of new particle formation during post monsoon season over a high-altitude site of the Western Ghats, India. *Toxicological & Environmental Chemistry*, 99(4), 652-664. <https://doi.org/10.1080/02772248.2016.1274031>

Magee Scientific (2016), Aethalometer® Model AE33 User Manual - Version 1.54. Aerosol d.o.o., Rep., 159-195 pp, Ljubljana, Slovenia.

Manninen, H. E., Nieminen, T., Asmi, E., Gagné, S., Häkkinen, S., Lehtipalo, K., Aalto, P., Vana, M., Mirme, A., Mirme, S., Hörrak, U., Plass-Dülmer, C., Stange, G., Kiss, G., Hoffer, A., Törö, N., Moerman, M., Henzing, B., de Leeuw, G., Brinkenberg, M., Kouvarakis, G. N., Bougiatioti, A., Mihalopoulos, N., O'Dowd, C., Ceburnis, D., Arneth, A., Svenningsson, B., Swietlicki, E., Tarozzi, L., Decesari, S., Facchini, M. C., Birmili, W., Sonntag, A., Wiedensohler, A., Boulon, J., Sellegrí, K., Laj, P., Gysel, M., Bukowiecki, N., Weingartner, E., Wehrle, G., Laaksonen, A., Hamed, A., Joutsensaari, J., Petäjä, T., Kerminen V.-M., & M. Kulmala (2010). EUCAARI ion spectrometer measurements at 12 European sites – analysis of new particle formation events. *Atmospheric Chemistry and Physics*, 10(16), 7907-7927. <https://doi.org/10.5194/acp-10-7907-2010>

McFiggans, G., Artaxo, P., Baltensperger, U., Coe, H., Facchini, M. C., Feingold, G., Fuzzi, S., Gysel, M., Laaksonen, A., Lohmann, U., Mentel, T. F., Murphy, D. M., O'Dowd, C. D., Snider, J. R., & Weingartner, E. (2006) The effect of physical and chemical aerosol properties on warm cloud droplet activation, *Atmospheric Chemistry and Physics*, 6, 2593–2649. <https://doi.org/10.5194/acp-6-2593-2006>

Mönkkönen, P., Koponen, I. K., Lehtinen, K. E. J., Hämeri, K., Uma, R., & Kulmala, M. (2005). Measurements in a highly polluted Asian mega city: observations of aerosol number size distribution, modal parameters and nucleation events. *Atmospheric Chemistry and Physics*, 5(1), 57-66. <https://doi.org/10.5194/acp-5-57-2005>

Moorthy, K. K., Sreekanth, V., Chaubey, J. P., Gogoi, M. M., Babu, S. S., Kompalli, S. K., Bagare, S. P., Bhuvan, C. Bhatt, B.C., Gaur, V. K., Prabhu, T. P., & Singh, N. S. (2011). Fine and ultrafine particles at a near-free tropospheric environment over the high-altitude station Hanle in the Trans-Himalaya: New particle formation and size distribution. *Journal of Geophysical Research: Atmospheres*, 116(D20), n/a-n/a. <https://doi.org/10.1029/2011JD016343>

Neitola, K., Asmi, E., Komppula, M., Hyvärinen, A. P., Raatikainen, T., Panwar, T. S., Sharma, V. P., & Lihavainen, H. (2011). New particle formation infrequently observed in Himalayan foothills – why?. *Atmospheric Chemistry and Physics*, 11(16), 8447-8458. <https://doi.org/10.5194/acp-11-8447-2011>

Nie, W., Ding, A., Wang, T., Kerminen, V-M., George, C., Xue, K., Wang, W., Zhang, Q., Petäjä, T., Qi, X., Gao, X., Wang, X., Yang, X., Fu, C., & Kulmala, M. (2014). Polluted dust

promotes new particle formation and growth. *Scientific Reports*, 4(1), 6634. <https://doi.org/10.1038/srep06634>.

Nieminan, T., Asmi, A., Maso, M. D., Aalto, P. P., Keronen, P., Petaja, T., Kulmala, M., and Kerminen, V-M. (2014). Trends in atmospheric new-particle formation: 16 years of observations in a boreal-forest environment. *Boreal Environment Research*, 19(B), 191-204. <http://hdl.handle.net/10138/165199>

Nieminan, T., Kerminen, V-M., Petäjä, T., Aalto, P. P., Arshinov, M., Asmi, E., Baltensperger, U., Beddows, D. C. S., Beukes, J. P., Collins, D., Ding, D., arrison, R. M., Henzing, B., Hooda, R., Hu, M., Hörrak, U., Kivekäs, N., Komsaare, K., Krejci, R., Kristensson, A., Laakso, L., Laaksonen, A., Leaitch, W. R., Lihavainen, H., Mihalopoulos, N., Németh, Z., Nie, W., O'Dowd, C., Salma, I., Sellegrí, K., Svenningsson, B., Swietlicki, E., Tunved, P., Ulevicius, V., Vakkari, V., Vana, M., Wiedensohler, A., Wu, Z., Virtanen, A., & Kulmala, M., (2018). Global analysis of continental boundary layer new particle formation based on long-term measurements. *Atmospheric Chemistry and Physics*, 18(19), 14737-14756. <https://doi.org/10.5194/acp-18-14737-2018>

Nilsson, E. D., Paatero, J., & Boy, M. (2001). Effects of air masses and synoptic weather on aerosol formation in the continental boundary layer, *Tellus B: Chemical and Physical Meteorology*, 53(4), 462-478. <https://doi.org/10.3402/tellusb.v53i4.16619>

Paasonen, P., Asmi, A. Petäjä, T., K. Kajos, M. K., Äijälä, M., Junninen, H., Holst, T., P. D. Abbatt, J. P., Arneth, A., Birmili, W., van der Gon, H. D., Hamed, A., Hoffer, A., Laakso, L., Laaksonen, A., Leaitch, W. R., Plass-Dülmer, C., Pryor, S. C., Räisänen, P., Swietlicki, E., Wiedensohler, A., Worsnop, D. R., Kerminen, V-M., & Kulmala, M. (2013). Warming-induced increase in aerosol number concentration likely to moderate climate change. *Nature Geoscience*, 6(6), 438-442. <https://doi.org/10.1038/ngeo1800>

A. Petzold, Ogren, J. A., Fiebig, M., Laj, P., Li, S.-M., Baltensperger, U., Holzer-Popp, T., Kinne, S., Pappalardo, G., Sugimoto, N., Wehrli, C., Wiedensohler, A., & Zhang, X-Y. (2013), Recommendations for reporting "black carbon" measurements, *Atmos. Chem. Phys.*, 13(16), 8365-8379. <https://doi.org/10.5194/acp-13-8365-2013>

Pierce, J. R., and P. J. Adams (2007). Efficiency of cloud condensation nuclei formation from ultrafine particles. *Atmospheric Chemistry and Physics*, 7(5), 1367-1379. <https://doi.org/10.5194/acp-13-8365-2013>

Pierce, J. R., Westervelt, D. M., Atwood, S. A., Barnes, E. A., & Leaitch, W. R. (2014). New-particle formation, growth and climate-relevant particle production in Egbert, Canada: analysis from 1 year of size-distribution observations. *Atmospheric Chemistry and Physics*, 14(16), 8647-8663. <https://doi.org/10.5194/acp-14-8647-2014>

Pierce, J. R., Leaitch, W. R., Liggio, J., Westervelt, D. M., Wainwright, C. D., Abbatt, J. P. D., Ahlm, L., Al-Basheer, W., Cziczo, D. J., Hayden, K. L., Lee, A. K. Y., Li, S.-M., Russell, L. M., Sjostedt, S. J., Strawbridge, K. B., Travis, M., Vlasenko, A., Wentzell, J. J. B., Wiebe, H. A., Wong, J. P. S., & Macdonald, A. M. (2012). Nucleation and condensational growth to CCN

sizes during a sustained pristine biogenic SOA event in a forested mountain valley. *Atmospheric Chemistry and Physics*, 12(7), 3147-3163. <https://doi.org/10.5194/acp-12-3147-2012>

Rose, C., Sellegrí, K., Velarde, F., Moreno, I., M. Ramonet, Weinhold, K., Krejci, R., Ginot, P., Wiedensohler, A., & Laj, P., (2015). Frequent nucleation events at the high altitude station of Chacaltaya (5240 m a.s.l.), Bolivia. *Atmospheric Environment*, 102, 18-29. <https://doi.org/10.1016/j.atmosenv.2014.11.015>

Rose, C., Sellegrí, K., Moreno, I., Velarde, F., Ramonet, M., Weinhold, K., Krejci, R., Andrade, M., Wiedensohler, A., Ginot, P. A. & Laj, P. (2017). CCN production by new particle formation in the free troposphere. *Atmospheric Chemistry and Physics*, 17(2), 1529-1541. <https://doi.org/10.5194/acp-17-1529-2017>

Rosenfeld, D., Sherwood, S., Wood, R., & Donner, L. (2014). Climate Effects of Aerosol-Cloud Interactions. *Science*, 343(6169), 379-380. <https://doi.org/10.1126/science.1247490>

Sarangi, C., Kanawade, V. P., Tripathi, S. N., Thomas, A., & Ganguly, D. (2018). Aerosol-induced intensification of cooling effect of clouds during Indian summer monsoon. *Nature Communications*, 9(1), 3754. <https://doi.org/10.1038/s41467-018-06015-5>

Sellegrí, K., Rose, C., Marinoni, A., Lupi, A., Wiedensohler, A., Andrade, M., Bonasoni, P., & Laj, P. (2019). New Particle Formation: A Review of Ground-Based Observations at Mountain Research Stations. *Atmosphere*, 10(9), 493. <https://doi.org/10.3390/atmos10090493>

Serafin, S., et al. (2018), Exchange Processes in the Atmospheric Boundary Layer Over Mountainous Terrain, *Atmosphere*, 9(102).

Shen, X. J., Sun, J., Zhang, X., Zhang, Y., Zhang, L., & Fan, R. (2016). Key features of new particle formation events at background sites in China and their influence on cloud condensation nuclei. *Frontiers of Environmental Science & Engineering*, 10(5), 5. <https://doi.org/10.1007/s11783-016-0833-2>

Shen, X. J., Sun, J. Y., Zhang, Y. M., Wehner, B., Nowak, A., Tuch, T., Zhang, X. C., Wang ,T. T., Zhou, H. G., Zhang, X. L., Dong, F., Birmili, W., & Wiedensohler, A. (2011). First long-term study of particle number size distributions and new particle formation events of regional aerosol in the North China Plain. *Atmospheric Chemistry and Physics*, 11(4), 1565-1580. <https://doi.org/10.5194/acp-11-1565-2011>

Singh, N., R. Solanki, N. Ojha, R. H. H. Janssen, A. Pozzer, and S. K. Dhaka (2016), Boundary layer evolution over the central Himalayas from radio wind profiler and model simulations, *Atmos. Chem. Phys.*, 16(16), 10559-10572.

Sogacheva, L., Maso, M. D., Kerminen, V.-M., & Kulmala, M. (2005). Probability of nucleation events and aerosol particle concentration in different air mass types arriving at Hyytiälä, southern Finland, based on back trajectory analysis. *Boreal Environment Research*, 10, 479–491.

Sogacheva, L., Hamed, A., Facchini, M. C., Kulmala, M., & Laaksonen, A. (2007). Relation of air mass history to nucleation events in Po Valley, Italy, using back trajectories analysis. *Atmospheric Chemistry and Physics*, 7(3), 839-853. <https://doi.org/10.5194/acp-7-839-2007>

Sullivan, R. C., Crippa, P., Matsui, H., Leung, L. R., Zhao, C., Thota, A., & Pryor, S. C. (2018). New particle formation leads to cloud dimming. *npj Climate and Atmospheric Science*, 1(1), 9. <https://doi.org/10.1038/s41612-018-0019-7>

Tröstl, J., Herrmann, E., Frege, C., Bianchi, F., Molteni, U., Bukowiecki, N. B., Hoyle, C. R., Steinbacher, M., Weingartner, E., Dommen, J., Gysel, M., & Baltensperger, U. (2016). Contribution of new particle formation to the total aerosol concentration at the high-altitude site Jungfraujoch (3580 m asl, Switzerland). *Journal of Geophysical Research: Atmospheres*, 121(19), 11,692-611,711. <https://doi.org/10.1002/2015JD024637>

Upadhyay, Ranjan, R. G., R., & Negi, P. S. (2015). Climate variability and trend at Ranichauri (Uttarakhand). *Journal of Agrometeorology*, 17(2), 241-243.

Venzac, H., Sellegrí K., Villani P., Picard D., & Laj P. (2009). Seasonal variation of aerosol size distributions in the free troposphere and residual layer at the puy de Dôme station, France, *Atmospheric Chemistry and Physics*, 9(4), 1465-1478. <https://doi.org/10.5194/acp-9-1465-2009>

Venzac, H., Sellegrí, K., Laj, P., Villani, P., Bonasoni, P., Marinoni, A., Cristofanelli, P., Calzolari, F., Fuzzi, S., De Cesari, S., Facchini, M-C., Vuillermoz, E., & Verza, G. P., (2008). High frequency new particle formation in the Himalayas. *Proceedings of the National Academy of Sciences*, 105(41), 15666-15671. <https://doi.org/10.1073/pnas.0801355105>

von Schneidemesser, E., Paul S. Monks, P. S., James D. Allan, J. D., Lori Bruhwiler, L., Piers Forster, P., David Fowler, D., Axel Lauer, A., William T. Morgan, W. T., Pauli Paasonen, P., Mattia Righi, M., Katerina Sindelarova, K., Mark A. & Sutton, M. A. (2015). Chemistry and the Linkages between Air Quality and Climate Change. *Chemical Reviews*, 115(10), 3856-3897. <https://doi.org/10.1021/acs.chemrev.5b00089>

Wang, M., & Penner, J. E. (2009). Aerosol indirect forcing in a global model with particle nucleation. *Atmospheric Chemistry and Physics*, 9(1), 239-260. <https://doi.org/10.5194/acp-9-239-2009>

Wang, Z., Birmili, W., Hamed, A., Wehner, B., Spindler, G., Pei, X., Wu, Z., Cheng, Y., Su, H., and Wiedensohler, A. (2017), Contributions of volatile and nonvolatile compounds (at 300°C) to condensational growth of atmospheric nanoparticles: An assessment based on 8.5 years of observations at the Central Europe background site Melpitz, *Journal of Geophysical Research: Atmospheres*, 122(1), 485-497, doi:<https://doi.org/10.1002/2016JD025581>

Westervelt, D. M., Pierce, J. R., & Adams, P. J. (2014). Analysis of feedbacks between nucleation rate, survival probability and cloud condensation nuclei formation. *Atmospheric Chemistry and Physics*, 14(11), 5577-5597. <https://doi.org/10.5194/acp-14-5577-2014>

Westervelt, D. M., Pierce, J. R., Riipinen, I., Trivitayanurak, W., Hamed, A., Kulmala, M., Laaksonen, A., De Cesari, S., & Adams, P. J. (2013). Formation and growth of nucleated

particles into cloud condensation nuclei: model–measurement comparison, *Atmospheric Chemistry and Physics*, 13(15), 7645-7663. <https://doi.org/10.5194/acp-13-7645-2013>

Wiedensohler, A., Birmili, W., Nowak, A., Sonntag, A., Weinhold, K., Merkel, M., Wehner, B., Tuch, T., Pfeifer, S., Fiebig, M., Fjäraa, A. M., Asmi, E., Sellegrí, K., Depuy, R., Venzac, H., Villani, P., Laj, P., Aalto, P., Ogren, J. A., Swietlicki, E., Williams, P., Roldin, P., Quincey, P., Hüglin, C., Fierz-Schmidhauser, R., Gysel, M., Weingartner, E., Riccobono, F., Santos, S., Grüning, C., Faloon, K., Beddows, D., Harrison, R., Monahan, C., Jennings, S. G., O'Dowd, C. D., Marinoni, A., Horn, H.-G., Keck, L., Jiang, J., Scheckman, J., McMurry, P. H., Deng, Z., Zhao, C. S., Moerman, M., Henzing, B., de Leeuw, G., Löschau, G., & Bastian, S. (2012). Mobility particle size spectrometers: harmonization of technical standards and data structure to facilitate high quality long-term observations of atmospheric particle number size distributions. *Atmospheric Measurement Techniques*, 5(3), 657-685. <https://doi.org/10.5194/amt-5-657-2012>

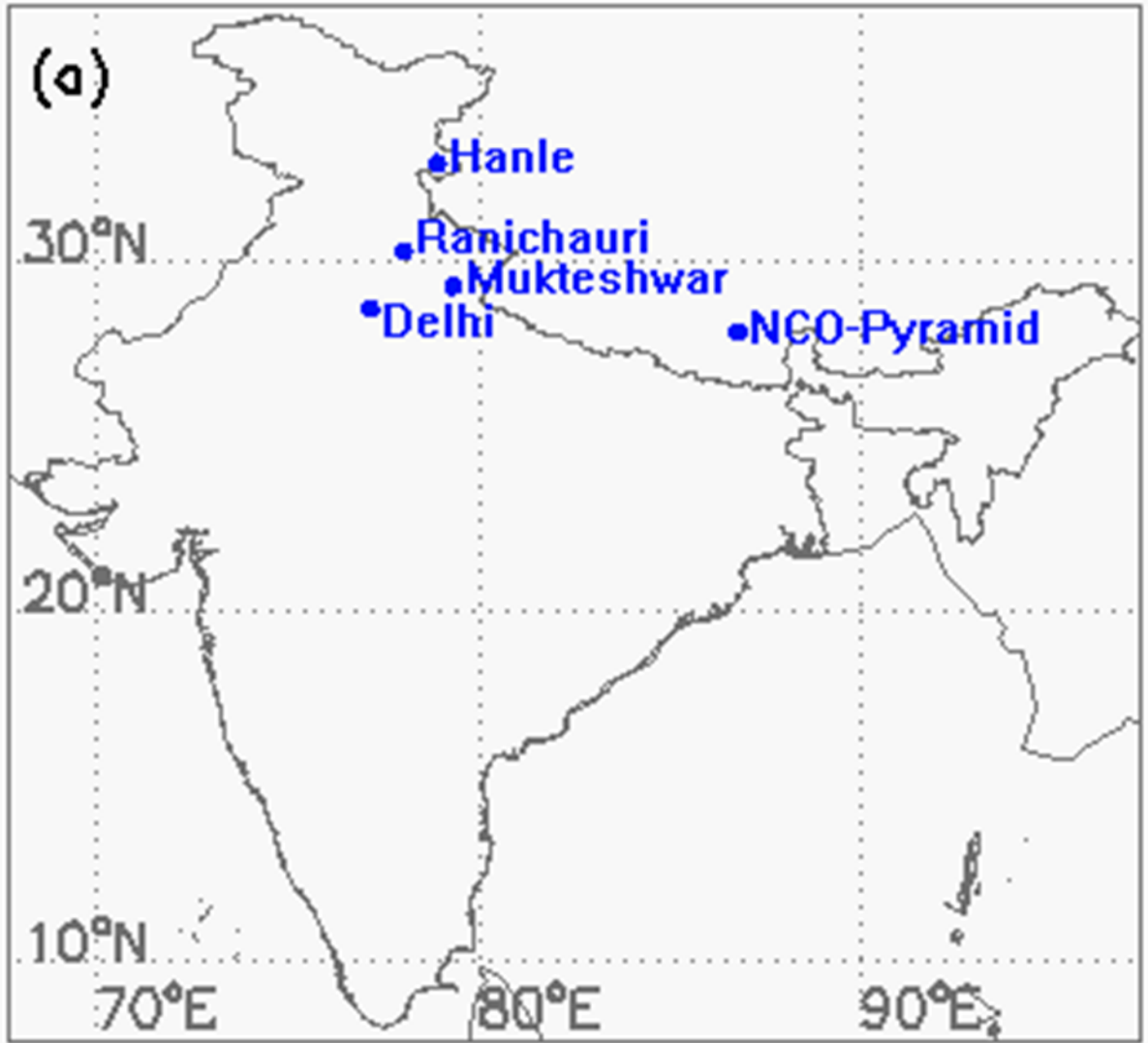
Yao, L., Garmash, O., Bianchi, F., Zheng, J., Yan, C., Kontkanen, J., Junninen, H., Mazon, S. B., Ehn, M., Paasonen, P., Sipilä, M., Wang, M., Wang, X., Xiao, S., Chen, H., Lu, Y., Zhang, B., Wang, D., Fu, Q., Geng, F., Li, L., Wang, H., Qiao, L., Yang, X., Chen, J., Kerminen, V.-M., Petäjä, T., Worsnop, D. R., Kulmala, M., & Wang, L. (2018). Atmospheric new particle formation from sulfuric acid and amines in a Chinese megacity. *Science*, 361(6399), 278-281. <https://doi.org/10.1126/science.aoa4839>

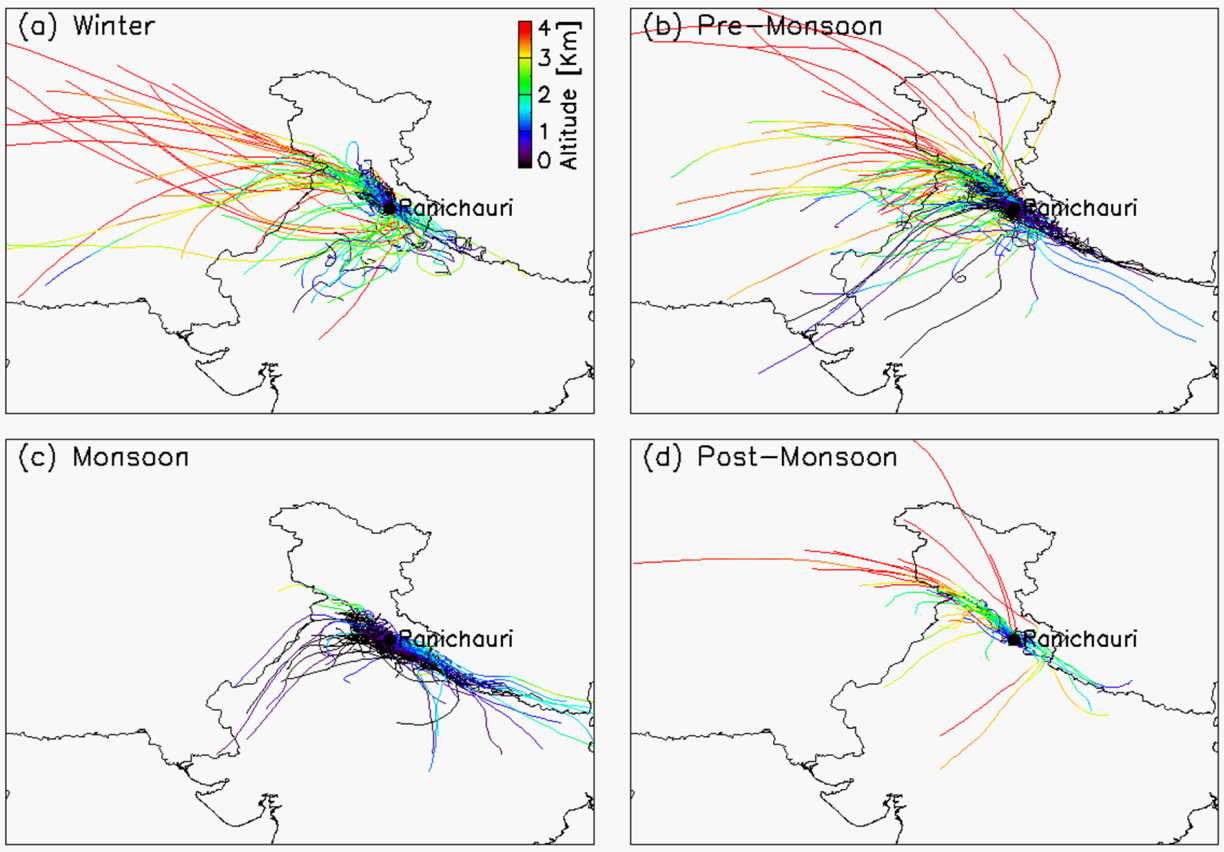
Yu, H., Ren, L., & Kanawade, V. P. (2017). New Particle Formation and Growth Mechanisms in Highly Polluted Environments. *Current Pollution Reports*, 3(4), 245-253. <https://doi.org/10.1007/s40726-017-0067-3>

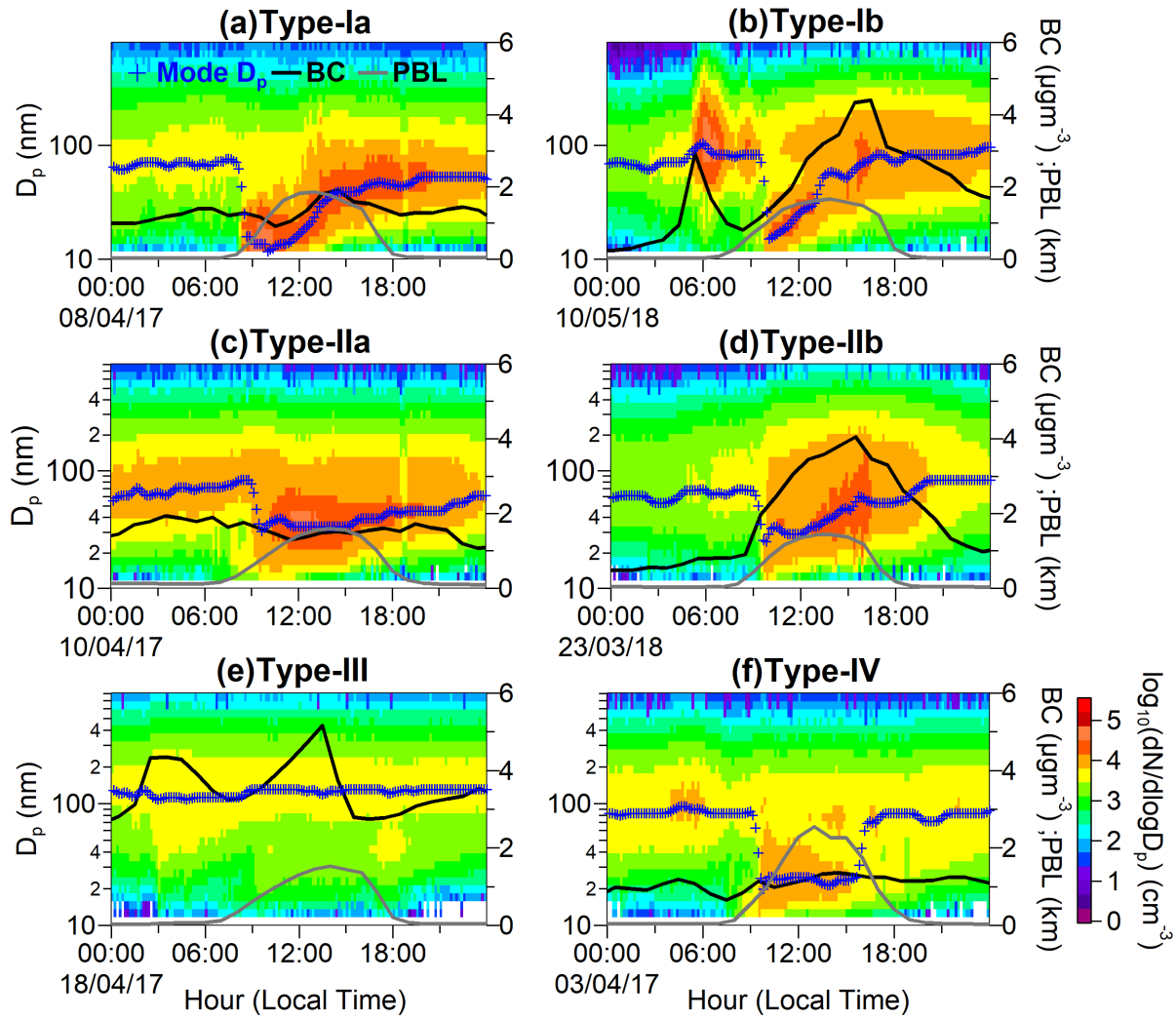
Zhang, R., Khalizov, A., Wang, L., Hu, M., & Xu, W. (2012). Nucleation and Growth of Nanoparticles in the Atmosphere. *Chemical Reviews*, 112(3), 1957-2011. <https://doi.org/10.1021/cr2001756>

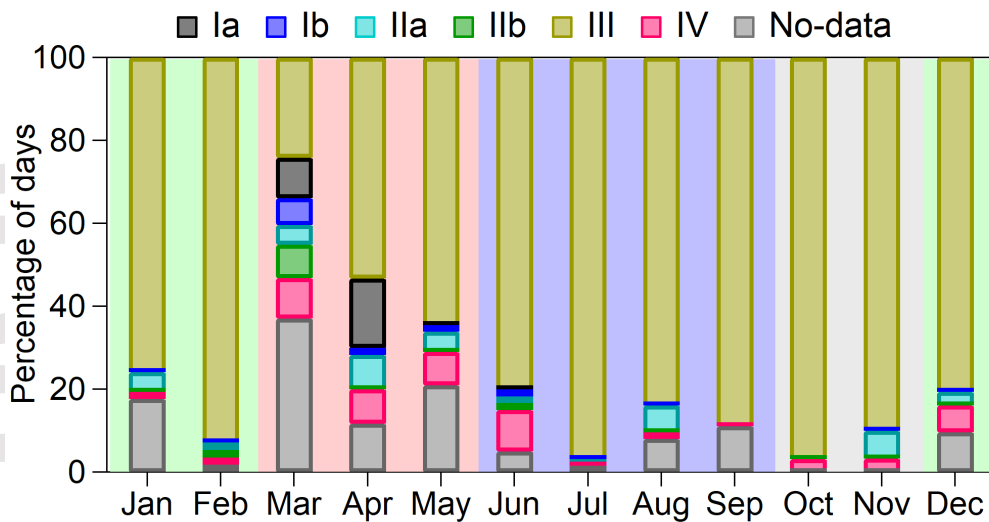
Zhang, R., Wang, G., Guo, S., Zamora, M. L., Ying, Q., Lin, Y., Wang, W., Hu, M., & Wang, Y. (2015). Formation of Urban Fine Particulate Matter. *Chemical Reviews*, 115(10), 3803-3855. <https://doi.org/10.1021/acs.chemrev.5b00067>

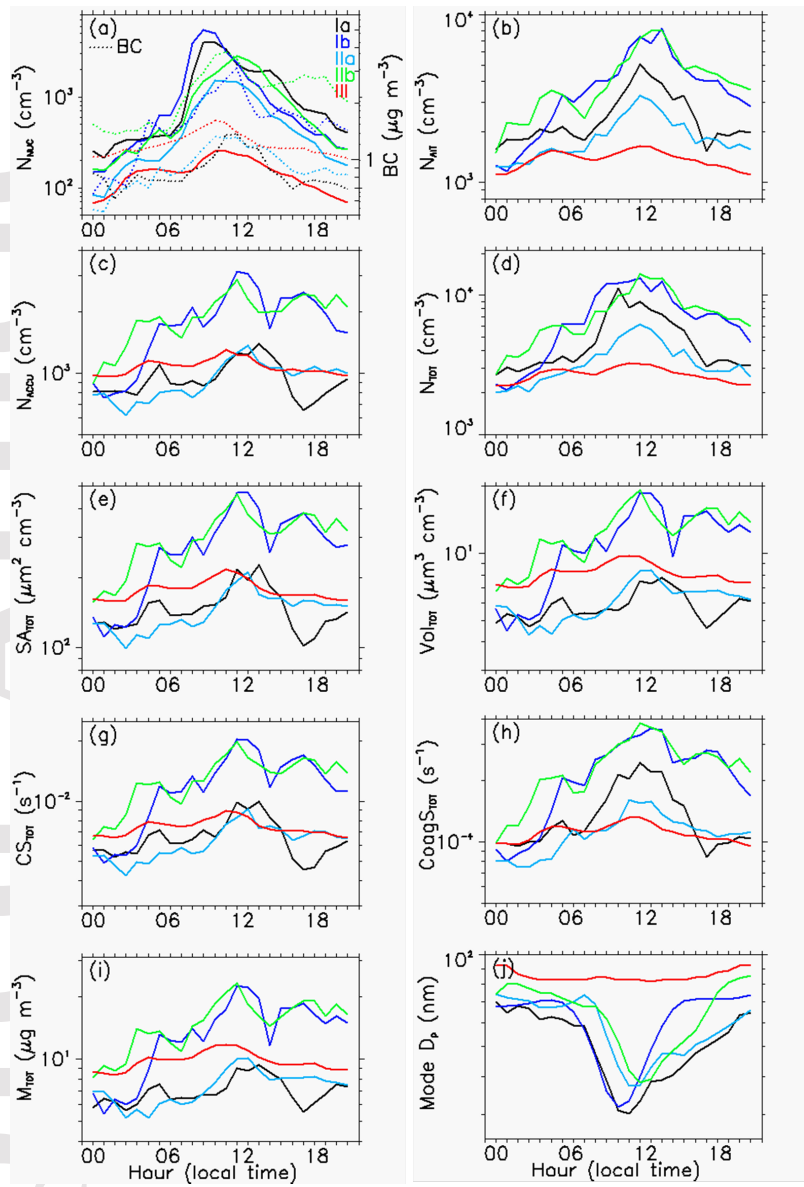
Zhu, Y., Xue, L., Gao, J., Chen, J., Li, H., Zhao, Y., Guo, Z., Chen, T., Wen, L., Zheng, P., Shan, Y., Wang, X., Wang, T., Yao, X., and Wang, W. (2020), Increased new particle yields with largely decreased probability of survival to CCN size at the summit of Mt. Tai under reduced SO₂ emissions, *Atmospheric Chemistry and Physics Discussions*, 2020, 1-30, doi: <https://doi.org/10.5194/acp-2020-364>

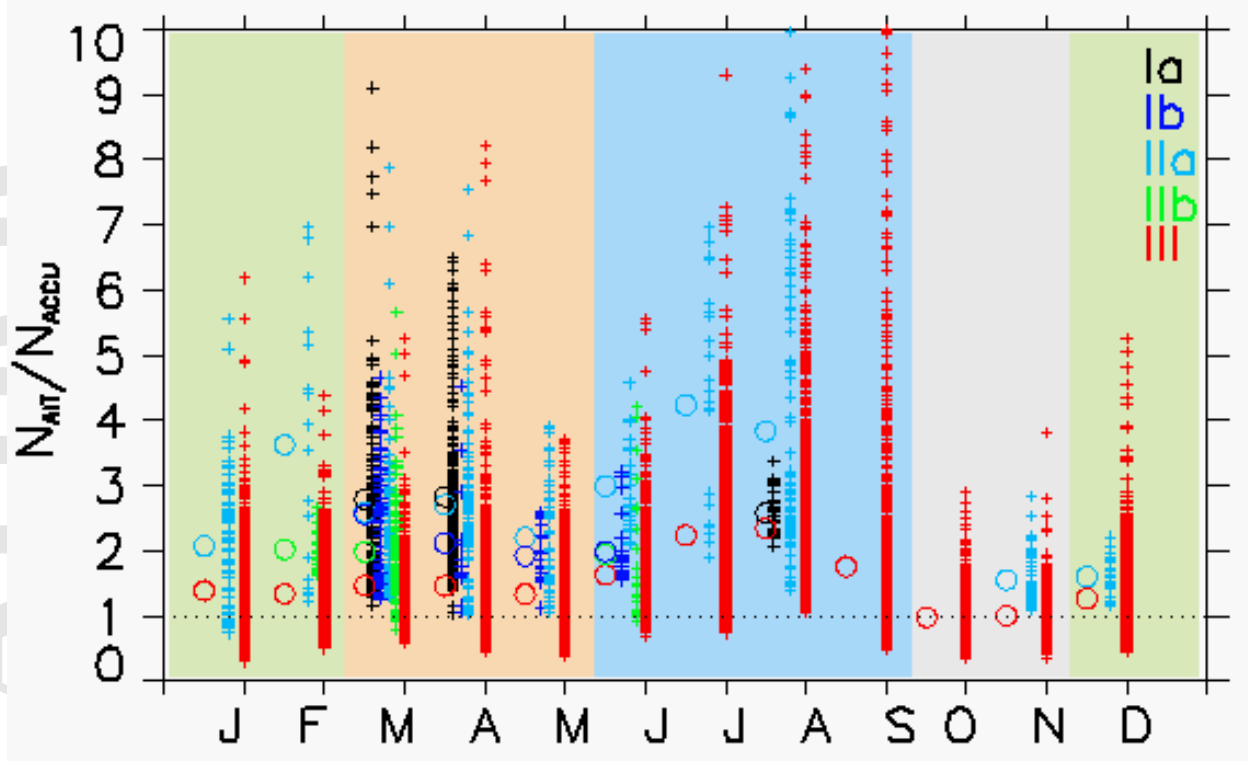


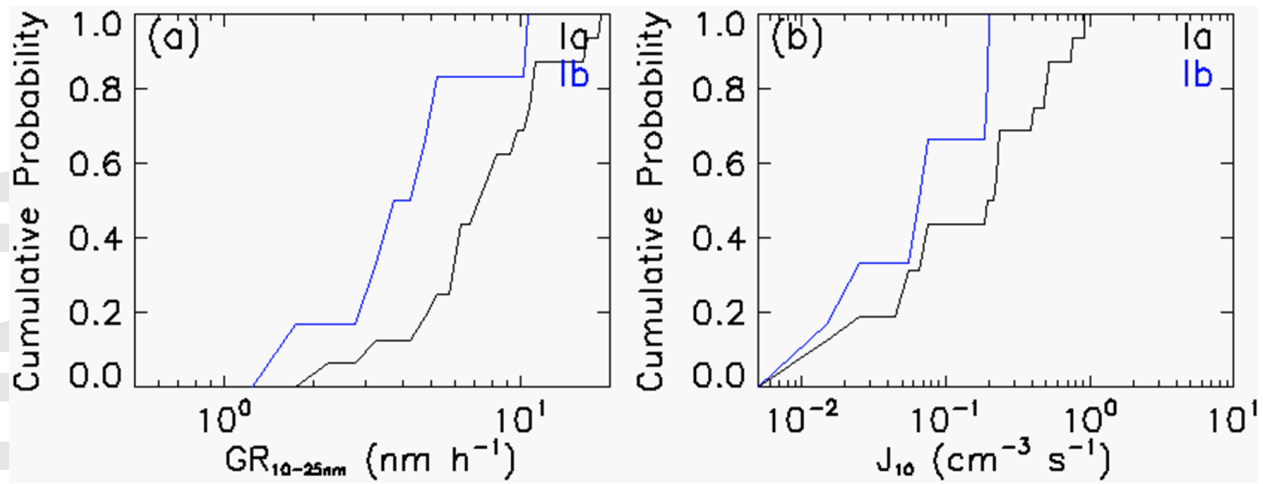


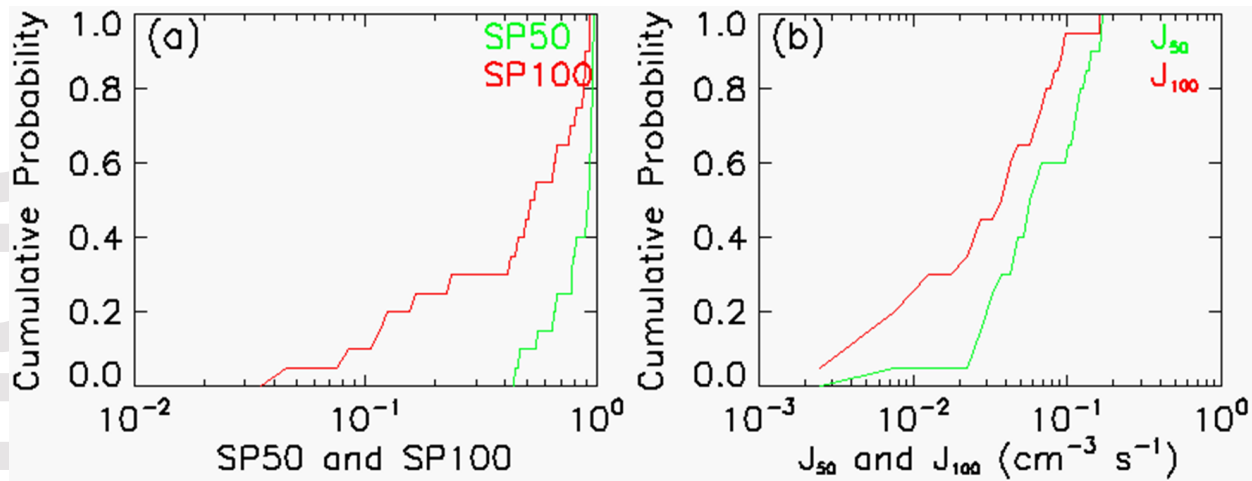




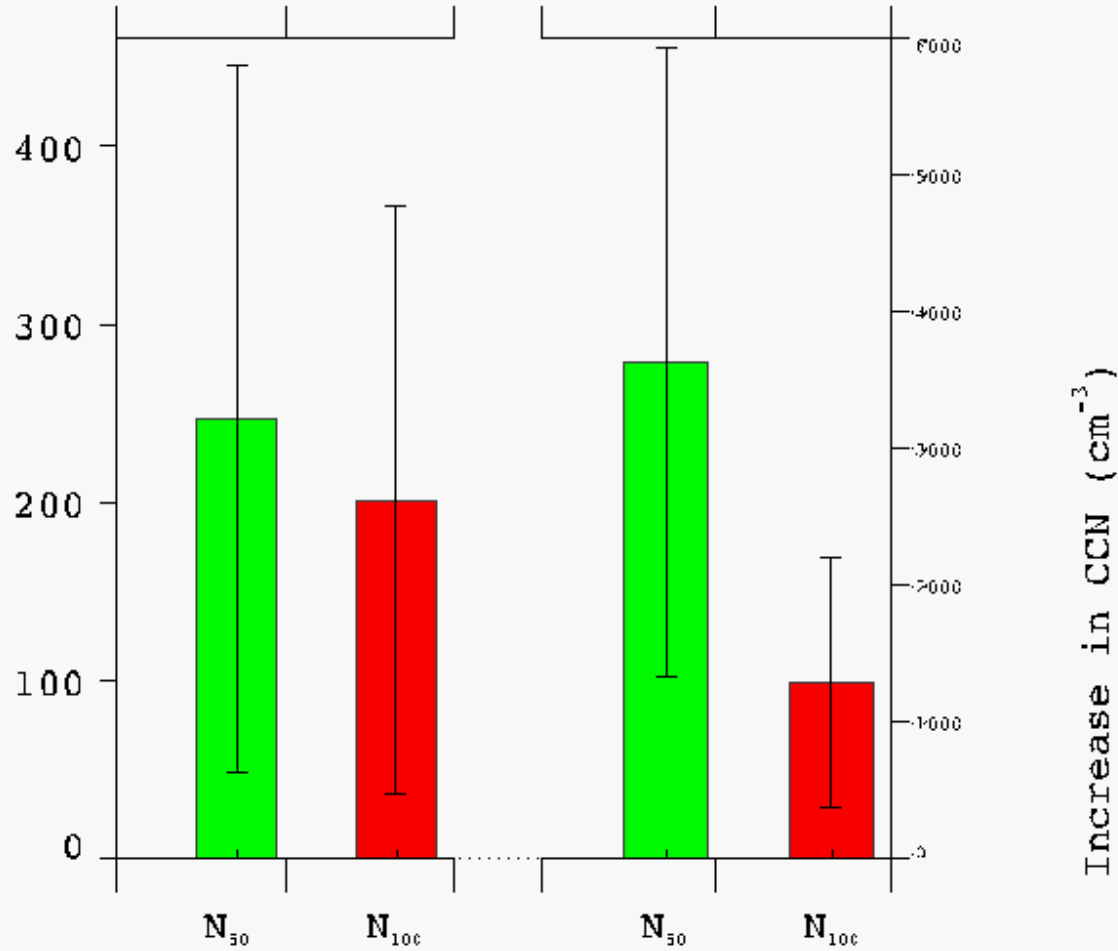








Increase in CCN (%)



[View publication stats](#)